On the modeling and simulation of of reaction-transfer dynamics in semiconductor-electrolyte solar cells

Yuan He* Irene M. Gamba† Heung-Chan Lee‡ Kui Ren§

April 16, 2013

Abstract

The mathematical modeling and numerical simulation of semiconductor-electrolyte systems play important roles in the design of high-performance semiconductor-liquid junction solar cells. We propose in this work a macroscopic mathematical model, a system of nonlinear partial differential equations, for the complete description of charges transfer dynamics in such systems. The model consists of a reaction-drift-diffusion-Poisson system that models the transport of electron-hole pairs in the semiconductor region and an equivalent system that describes the transport of reductant-oxidant pairs in the electrolyte region. The coupling between the semiconductor and the electrolyte is modeled through a set of interfacial reactive and current balance conditions. We present some numerical simulations to illustrate the quantitative behavior of the semiconductor-electrolyte system in both dark and illuminated environments. We show numerically that one can replace the electrolyte region in the system with a Schottky contact only when the bulk reductant-oxidant pair density is extremely high. Otherwise, such replacement gives significantly inaccurate description of the real dynamics of the semiconductor-electrolyte system.

Key words. Semiconductor-electrolyte system, reaction-drift-diffusion-Poisson system, semiconductor modeling, interfacial charge transfer, interface conditions, semiconductor-liquid junction, solar cell simulation, naso-scale device modeling.

1 Introduction

The mathematical modeling and simulation of semiconductor devices have been extensively studied in the past decades due to its importance in industrial applications; see [2, 29, 33, 36, 39, 45, 46, 44, 63, 78, 80] for overviews of the field and [8, 34, 77, 90] for more details on

*ICES,University of Texas, Austin, TX 78712; Email: yuan@ices.utexas.edu .

†Department of Mathematics and ICES, University of Texas, Austin, TX 78712; Email: gamba@math.utexas.edu .

‡Department of Chemistry, University of Texas, Austin, TX 78712; Email: hclee@austin.utexas.edu .

§Department of Mathematics, University of Texas, Austin, TX 78712; Email: ren@math.utexas.edu .

the physics, classical and quantum, of semiconductor devices. In the recent years, the field is boosted significantly by the increasing need of simulation tools for designing efficient solar cells to harvest sunlight for clean energy. Various theoretical and computational results on traditional semiconductor device modeling are revisited and modified to account for new physics in solar cell applications. We refer interested reader to [27] for a summary of various types of solar cells that have been constructed, [41, 55, 65] for simplified analytical solvable models that have been developed, and [18, 74, 51, 19, 32] for more advanced mathematical and computational analysis on various models. Mathematical modeling and simulation provide ways not only to improve our understanding on the behavior of the solar cells under experimental conditions, but also to predict the performance of solar cells with general device parameters and thus enable us to optimize the performance of the cells by selecting the optimal combination of these parameters.

One popular type of solar cells, besides those made of semiconductor p-n junctions, are cells made of semiconductor-liquid junctions. A typical liquid-junction photovotaic solar cell consists of four major components: the semiconductor, the liquid, the semiconductor-liquid interface and the counter electrode; see a rough sketch in Fig. 1. Different semiconductor-liquid combinations can be utilized, see for instance [27, Tab. 1]. The working mechanism of this type of cells is as follows. When sunlight is absorbed by the semiconductor, electron-hole pairs are generated. These electrons and holes are then separated by an applied potential gradient across the device. The separation of the electrons and holes leads to electrical current in the cell and concentration of charges on the semiconductor-liquid interface where electrochemical reactions and charge transfer occur.

The physics of charges transport in semiconductor-liquid junctions has been studied in the past by many investigators; see [50] for a recent review. The mechanisms of charge generation, recombination and transport in both the semiconductor and the liquid are now well-understood. However, the reaction and charge transfer process on the semiconductor-liquid interface is far less understood despite the extensive recent investigations from both the physical [30, 31, 48, 49, 68, 93] and the numerical simulation [65, 84] perspectives. The objective of this work is to mathematically model this interfacial charge transfer process so that we could derive a complete system of equations to describe the whole charge transport process in the semiconductor-liquid junction.

To be specific, we consider here semiconductor-liquid junction with the liquid being electrolyte that contains reductants r and oxidants o with charge numbers α_r and α_o respectively. We denote by $\Omega \subset \mathbb{R}^d$ $(d = 1, 2, 3)$ the domain of the interest which contains the semiconductor part Ω_{S} and the electrolyte part Ω_{E}. We denote by $\Sigma \equiv \partial\Omega_{\mathsf{E}} \cap \partial\Omega_{\mathsf{S}}$ the interface between the semiconductor and electrolyte, $\Gamma_{\mathsf{S}} = \partial\Omega \cap \partial\Omega_{\mathsf{S}}$ the part of semiconductor boundary that is not in contact with the electrolyte, and $\Gamma_{\mathsf{E}} = \partial\Omega \cap \partial\Omega_{\mathsf{E}}$ the part of electrolyte that is not in contact with the semiconductor. We denote by Σ_+ and Σ_- the semiconductor and the electrolyte sides of Σ respectively, and by $\boldsymbol{\nu}(\mathbf{x})$ the unit outer normal vector at $\mathbf{x} \in \partial\Omega_{\mathsf{S}}$. Thus on the interface Σ, $\boldsymbol{\nu}(\mathbf{x})$ points toward the electrolyte.

The mathematical modeling of the semiconductor-electrolyte system consists of three components: the model for the dynamics of electron and holes in the semiconductor Ω_{S}, the model for the dynamics of the reductants and oxidants in the electrolyte Ω_{E}, and the *reaction-transfer dynamics on the interface* Σ. Boundary conditions on the Γ_{S} and Γ_{E} are

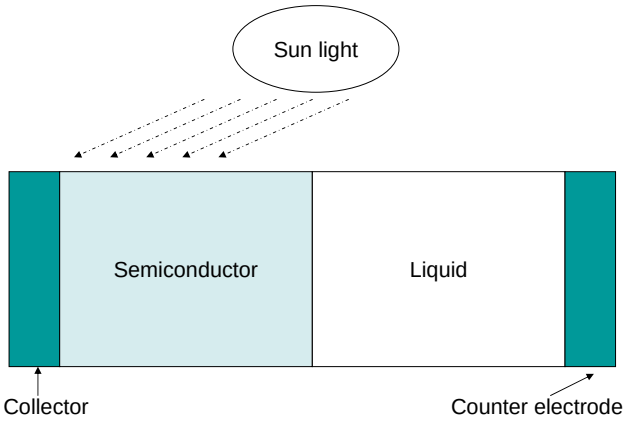

Figure 1: Sketch of the main components in a typical semiconductor-liquid junction solar cell.

specified by specific applications. For applications in solar cells, we have to also consider the generation of electron-hole pairs in the the semiconductor Ω_{S} due to the illumination by sunlight.

The rest of the paper is structured as follows. In Section 2 we first introduce the mathematical model for the transport of electron-hole pairs in the semiconductor. We then present the mathematical model for the dynamics of redox pairs in the electrolyte in Section 3. In Section 4 we present the interface conditions for densities and electrical field on the semiconductor-electrolyte interface. Numerical schemes for the solution of the system in simplified setting are presented in Section 5 and some numerical simulations are shown in Section 6 where we exhibit the benefits of modeling the complete semiconductor-electrolyte system. Concluding remarks are offered in Section 7.

2 Transport of electrons and holes

The modeling of transport of electrons and holes in semiconductor devices has been well-studied in the past decades [2, 29, 33, 36, 39, 63, 78, 80]. Many different models have been proposed, such as the Boltzmann-Poisson system [6, 11, 17, 20, 26, 37, 39, 61, 67, 75], the energy transport system [15, 23, 28, 39, 89, 82] and the drift-diffusion-Poisson system [1, 4, 12, 13, 22, 21, 38, 63, 62, 74, 76, 81, 85, 88]. For the purpose of computational efficiency, we employ the reaction-drift-diffusion-Poisson model in this work. Let us denote by $\mathbb{T} = (0, T]$ the time interval that we are interested in. The bipolar drift-diffusion-Poisson model can be written in the following form

$$\begin{aligned} \partial_t \rho_n + \nabla \cdot \mathbf{J}_n &= R_{np}(\rho_n, \rho_p) + \gamma G_{np}(\mathbf{x}), \quad \text{in} \quad (0,T] \times \Omega_{\mathsf{S}} \\ \partial_t \rho_p + \nabla \cdot \mathbf{J}_p &= R_{np}(\rho_n, \rho_p) + \gamma G_{np}(\mathbf{x}), \quad \text{in} \quad (0,T] \times \Omega_{\mathsf{S}} \\ -\nabla \cdot (\epsilon_r^{\mathsf{S}} \nabla \Phi) &= \frac{q}{\epsilon_0}[C(\mathbf{x}) + \rho_p - \rho_n], \quad \text{in} \quad (0,T] \times \Omega_{\mathsf{S}}. \end{aligned} \tag{1}$$

with the current densities of electrons and holes are given respectively by

$$\begin{aligned} \mathbf{J}_n &= -D_n \nabla \rho_n + \mu_n \rho_n \nabla \Phi, \\ \mathbf{J}_p &= -D_p \nabla \rho_p - \mu_p \rho_p \nabla \Phi. \end{aligned} \tag{2}$$

Here $\rho_n(t,\mathbf{x})$ and $\rho_p(t,\mathbf{x})$ are the densities of the electrons and holes at time t and location $\mathbf{x}$ respectively and $\Phi(t,\mathbf{x})$ is the electrical potential. The notation ∂_t denotes the derivative with respect to t while ∇ denotes the usual spatial gradient operator. The constant ϵ_0 is the dielectric constant in vacuum and the function $\epsilon_r^{\mathsf{S}}(\mathbf{x})$ is the relative dielectric function of the semiconductor material. The function $C(\mathbf{x})$ is the doping profile of the device. The coefficients D_n (resp. D_p) and μ_n (resp. μ_p) are the diffusivity and the mobility of electrons (resp. holes). These parameters can be computed from the first principles of statistical physics. In some practical applications, however, they can be fitted from experimental data as well; see for example the discussion in [77]. The parameter q is the unit electric charge constant. The diffusivity and the mobility coefficients are related through the Einstein relations $D_n = U_{\mathcal{T}}\mu_n$ and $D_p = U_{\mathcal{T}}\mu_p$ with $U_{\mathcal{T}}$ the thermal voltage at temperature $\mathcal{T}$ given by $U_{\mathcal{T}} = k_B\,\mathcal{T}/q$, k_B being the Boltzmann constant.

2.1 Charge generation and recombination

The function $R_{np}(\rho_n,\rho_p)$ is the generation-recombination rate, in other words, the rate at which electron-hole pairs are generated subtracted by the rate at which electron-hole pairs are recombined. Since electrons and holes are generated and recombined in pairs, we have the same rate function for the two species. We consider in this work two types of generation-recombination models. The first one is the Auger model [63]. It is given by

$$R_{np}(\rho_n,\rho_p) = (A_n\rho_n + A_p\rho_p)(\rho_i^2 - \rho_n\rho_p), \tag{3}$$

where A_n and A_p are the Auger coefficients for electrons and holes respectively. For given materials, A_n and A_p can be measured by experiments. The parameter ρ_i is the intrinsic carrier density that is often calculated from the following formula [42]

$$\rho_i = \sqrt{N_c N_v}\left(\frac{\mathcal{T}}{300}\right)^{1.5} e^{-E_g/(2k_B\mathcal{T})} \tag{4}$$

where the band gap at temperature $\mathcal{T}$, $E_g = E_{g0} - \alpha\mathcal{T}^2/(\mathcal{T}+\beta)$ with E_{g0} the band gap at $\mathcal{T} = 0K$ ($E_{g0} = 1.17q$ for silicon for instance), $\alpha = 4.73\ 10^{-4}q$, and $\beta = 636$. The parameters N_c and N_v are effective density of states in the conduction and the valence bands respectively at $\mathcal{T} = 300K$.

The second generation-recombination model we consider is the Shockley-Read-Hall (SRH) model [63]. It reads

$$R_{np}(\rho_n,\rho_p) = \frac{\rho_i^2 - \rho_n\rho_p}{\tau_p(\rho_n+\rho_i) + \tau_n(\rho_p+\rho_i)}, \tag{5}$$

where the coefficients τ_n and τ_p are the life time parameters for electrons and holes respectively. The values of these parameters are provided in Tab. 1 in Section 6.

When the semiconductor device is illuminated under the sun light, the device absorbs photon energy, and electrons and holes can then be generated. This generation of charges is modeled by the source function $G_{np}(\mathbf{x})$ in the transport equation (1). Once again, due to the fact that electrons and holes are always generated in pairs, the generating functions are the same for electrons and holes. We take a model that assumes that photons travel across the device in straight lines. That is, we assume that photons do not get scattered

by the semiconductor material during their travel inside the device. This is a reasonable assumption for small devices that have been utilized widely [40]. Precisely, the generation of charges is given as

$$G_{np}(\mathbf{x}) = \begin{cases} \sigma(\mathbf{x})G_0(\mathbf{x}_0)e^{-\int_0^s \sigma(\mathbf{x}_0+s'\boldsymbol{\theta}_0)ds'}, & \text{if } \mathbf{x} = \mathbf{x}_0 + s\boldsymbol{\theta}_0 \\ 0, & \text{otherwise} \end{cases} \tag{6}$$

where $\mathbf{x}_0$ is the incident location, $\boldsymbol{\theta}_0$ is the incident direction, $\sigma(\mathbf{x})$ is the absorption coefficient (integrated over usable wavelengths), and $G_0(\mathbf{x}_0)$ is the surface photon flux at $\mathbf{x}_0$. The control parameter $\gamma \in \{0,\ 1\}$ in (1) is used to turn on and off the illumination mechanism. The cases of $\gamma = 0$ and $\gamma = 1$ are called dark and illuminated respectively in solar cell research community.

2.2 Boundary conditions

There are mainly two types of boundary conditions for the simulation in the semiconductor part, depending on material we put in contact with the semiconductor: Dirichlet boundary conditions at Ohmic contact and Neuman boundary conditions at Schottky contact. We denote from now on $\Gamma_{\mathsf{S}o}$ and $\Gamma_{\mathsf{S}s}$ the Ohmic and Schottky parts of the semiconductor boundary respectively. We have $\Gamma_{\mathsf{S}} = \Gamma_{\mathsf{S}o} \cup \Gamma_{\mathsf{S}s}$.

Dirichlet at Ohmic contacts. Ohmic contacts are used to model metal-semiconductor junctions that do not rectify current. This type of contacts are mainly used to carry electrical current out and into semiconductor devices, and should be fabricated with little (or ideally no) parasitic resistance. Low resistivity Ohmic contacts are also essential for high-frequency operation. Mathematically, Ohmic contacts are modeled by Dirichlet boundary conditions which can be written as

$$\begin{aligned} &\rho_n(t,\mathbf{x}) = \rho_n^e(\mathbf{x}), \qquad \rho_p(t,\mathbf{x}) = \rho_p^e(\mathbf{x}), \quad \text{on} \quad (0,T] \times \Gamma_{\mathsf{S}o}, \\ &\Phi(t,\mathbf{x}) = \varphi_{bi} + \varphi_{app}, \qquad\qquad\qquad\quad \text{on} \quad (0,T] \times \Gamma_{\mathsf{S}o}, \end{aligned} \tag{7}$$

where φ_{bi} and φ_{app} are the built-in and applied potential, respectively. The boundary values ρ_n^e, ρ_p^e for the Ohmic contacts are calculated following the assumptions that the semiconductor is in stationary and equilibrium state and the charge neutrality condition holds. This means that right-hand-side of the Poisson equation disappears so that

$$C + \rho_p^e - \rho_n^e = 0. \tag{8}$$

Thermal equilibrium implies that the generation-recombination balance out so $R = 0$ at Ohmic contacts. This leads to the mass-action law, between the density of electrons and holes:

$$\rho_n^e \rho_p^e - \rho_i^2 = 0. \tag{9}$$

The system of equations (8) and (9) admit a unique solution pair (ρ_n, ρ_p) which is given by

$$\begin{aligned} \rho_n^e(t,\mathbf{x}) &= \frac{1}{2}(\sqrt{C^2 + 4\rho_i^2} + C), \\ \rho_p^e(t,\mathbf{x}) &= \frac{1}{2}(\sqrt{C^2 + 4\rho_i^2} - C). \end{aligned} \tag{10}$$

These densities result in a built-in potential that can be calculated as

$$\varphi_{bi} = U_{\mathcal{T}} \ln(\rho_n^e/\rho_i). \tag{11}$$

Note that due to the fact that the doping profile C varies in space, these boundary values are different on different part of the boundary.

Robin (or Mixed) at Schottky contacts. More realistic metal-semiconductor junctions have rectifying effects in the sense that current flow through the contacts are rectified. Schottky contacts are more realistic models of this type of metal-semiconductor junctions. Mathematically, at Schottky contact, Robin (also called mixed) type of boundary conditions are imposed for the n- and p-components while Dirichlet type of conditions are imposed for the Φ-component. More precisely, these boundary conditions are:

$$\begin{array}{lll} \boldsymbol{\nu}\cdot\mathbf{J}_n(t,\mathbf{x}) = v_n(\rho_n-\rho_n^e)(\mathbf{x}), \quad \boldsymbol{\nu}\cdot\mathbf{J}_p(t,\mathbf{x}) = v_p(\rho_p-\rho_p^e)(\mathbf{x}), & \text{on} & (0,T]\times\Gamma_{\mathsf{S}s}, \\ \Phi(t,\mathbf{x}) = \varphi_{Schottky}+\varphi_{app}, & \text{on} & (0,T]\times\Gamma_{\mathsf{S}s}. \end{array} \tag{12}$$

Here the parameters for the Schottky barrier are the recombination velocities v_n and v_p, and the height of the potential barrier, $\varphi_{Schottky}$ which depends on the materials of the semiconductor and the metal in the following way:

$$\varphi_{Schottky} = \begin{cases} \Phi_m - \chi, & \text{n-type} \\ \dfrac{E_g}{q} - (\Phi_m - \chi), & \text{p-type} \end{cases} \tag{13}$$

where Φ_m is the work function, i.e., the potential difference between the Fermi energy and the vacuum level, of the metal and χ is the electron affinity, i.e., the potential difference between the conduction band edge and the vacuum level. E_g is again the band gap. The values of the parameters $v_n,\ v_p,\ \Phi_m$, and χ are given in Tab. 1 of Section 6.

We finish this section by the following remark. It is generally believed that the Boltzmann-Poisson model [39] is a more accurate model for charges transport in semiconductors. However, the Boltzmann-Poisson model is computationally more expensive to solve and analytically more complicated to analyze. The drift-diffusion-Poisson model (1) can be regarded as a macroscopic approximation to the Boltzmann-Poisson model. The validity of the drift-diffusion-Poisson model can be justified in the case when the mean free path of the charges is very small compared to the size of the device and the potential drop across the device is small (so that the electric field is not strong); see for instance [7, 10, 13, 14, 38] for such a justification.

3 Transport of reductants and oxidants

We now present the equations for the reaction-transport dynamics of reductant-oxidant (redox) pairs in the electrolyte. In principle, this dynamics is very similar to the electron-holes dynamics in the semiconductor. The main physical processes involved are reaction, recombination, transport and diffusion of the redox pairs. The dynamics can be modeled again with a set of reaction-drift-diffusion-Poisson equations, even though the mathematical

description of the dynamics is often called the Poisson-Nernst-Planck theory in the literature [24, 25, 35, 56, 58, 59, 64, 60, 79, 83, 86, 92]. Here we generalize the theory slightly to accommodate the specifics of our problem.

Let us denote by $\rho_r(t,\mathbf{x})$ the density of the reductants, and $\rho_o(t,\mathbf{x})$ the density of the oxidants. Then $(\rho_r(t,\mathbf{x}),\rho_o(t,\mathbf{x}))$ solves the following system that is of the same form as (1):

$$\begin{aligned}
&\partial_t\rho_r+\nabla\cdot\mathbf{J}_r=R_{ro}(\rho_r,\rho_o), && \text{in } (0,T]\times\Omega_{\mathsf{E}},\\
&\partial_t\rho_o+\nabla\cdot\mathbf{J}_o=-R_{ro}(\rho_r,\rho_o), && \text{in } (0,T]\times\Omega_{\mathsf{E}},\\
&-\nabla\cdot\epsilon_r^{\mathsf{E}}\nabla\Phi=\frac{q}{\epsilon_0}(\widehat{C}(\mathbf{x})+\alpha_o\rho_o-\alpha_r\rho_r), && \text{in } (0,T]\times\Omega_{\mathsf{E}}.
\end{aligned} \tag{14}$$

with the oxidant and reductant current densities given respectively by

$$\mathbf{J}_r=-D_r\nabla\rho_r+\mu_r\rho_r\nabla\Phi,\qquad \mathbf{J}_o=-D_o\nabla\rho_o-\mu_o\rho_o\nabla\Phi. \tag{15}$$

where again the diffusion coefficient D_r (resp. D_o) is related to the mobility μ_r (resp. μ_o) through the Einstein relation $D_r=U_{\mathcal{T}}\mu_r$ (resp. $D_o=U_{\mathcal{T}}\mu_o$). The parameters α_o and α_r are charge numbers of the oxidant and reductant respectively. Depending on the type of the redox pairs in the electrolyte, the charge numbers can be different. We refer interested reader to [27] for a summary of various types of redox pairs that have been developed in the past. The background $\widehat{C}$ is used here to take into account the general effect of the electrolyte on the transport dynamics of the redox pairs. In general cases, the electrolyte is neutral in charge, so we set $\widehat{C}=0$.

3.1 Charge generation through reaction

The reaction mechanism, modeled by the function R_{ro}, depends on the types of the reductants and the oxidants as well as the density of the redox pairs in the electrolyte. Note that the generation and elimination of reductant and oxidant pairs are very different from these of the electrons and holes. A oxidant is generated (resp. eliminated) when a reductant is eliminated (resp. generated) and vice versa. This is the reason why there is a negative sign in front of the function R_{ro} in the second equation of (14). For solar cell applications, it is usually true that the redox pair is very dilute in the electrolyte, with densities several order of magnitude smaller than the background charge densities in the electrolyte. Thus the reaction and recombination effect is extremely small. It is practical to assume that

$$R_{ro}(\rho_r,\rho_o)=0 \tag{16}$$

in general settings. This is what we adopt in the simulation of Section 6.

3.2 Boundary conditions

It is generally assumed that the interface of semiconductor and electrolyte is very far from the physical boundary of the electrolyte so that we can put an artificial boundary for the electrolyte system in the simulation. The boundary conditions for the redox pairs on the interface is thus set as their bulk values. Mathematically, this means that Dirichlet boundary

conditions have to be imposed for the reducant-oxidant pair. More precisely, we supply the following boundary condition for the drift-diffusion-Poisson system (14):

$$\rho_r(t,\mathbf{x}) = \rho_r^\infty(\mathbf{x}), \quad \rho_o(t,\mathbf{x}) = \rho_o^\infty(\mathbf{x}), \quad \Phi(t,\mathbf{x}) = \varphi_{bi}^{\mathsf{E}} + \varphi_{app}^{\mathsf{E}}, \quad \text{on} \quad (0,T]\times\Gamma_{\mathsf{E}} \tag{17}$$

where ρ_r^∞ and ρ_o^∞ are bulk concentration of the respective species, and $\varphi_{bi}^{\mathsf{E}}$ and $\varphi_{app}^{\mathsf{E}}$ are the built-in potential of electrolyte and the applied potential on the counter electrode respectively. The values of these parameters are given in Tab. 1 in Section 6.

Let us finish this section by the following remark. In the modeling of the dynamics of reductant-oxidant pair, we have implicitly assumed that the electrolyte, in which the redox pairs live, is not perturbed by charge motions. In other words, there is no macroscopic deformation of the electrolyte that can occur. If this is not the case, we have to introduce the equations of fluid dynamics, mainly the Navier-Stokes equation, for the fluid motion. The dynamics will thus be far more complicated.

4 Interfacial reaction and charge transfer

In order to obtain a complete mathematical model for the semiconductor-electrolyte system, we have to couple the system of equations for the electron-hole pairs in the semiconductor with the system of equations for the redox pair in the electrolyte. The coupling is through interface conditions on the semiconductor-electrolyte interface that describe the interfacial charge generation and transfer dynamics.

While there is a vast literature in physics and chemistry devoted to the study of microscopic electrochemical process on semiconductor-electrolyte interface [5, 30, 31, 40, 48, 49, 50, 65, 68, 69, 70, 71, 72, 73, 84, 93], we are only interested in deriving macroscopic interface conditions that are consistent with the dynamics of charge transport in the semiconductor and the electrolyte modeled by the equation systems (1) and (14). On that level, the reaction and charge transfer on the semiconductor-electrolyte interface can be described by the following first-order reaction and transfer relation

$$\mathrm{Ox} + e(\mathsf{S}) \rightleftharpoons \mathrm{Red} + \mathsf{S}, \tag{18}$$

where Ox and Red denote oxidant and reductant respectively, S denotes the semiconductor and $e(\mathsf{S})$ denotes an electron from the semiconductor. Then on the electrolyte side of the semiconductor-electrolyte interface, Σ_+, the changes of the concentrations of the redox pairs can be written as

$$\frac{d\rho_r}{dt} = k_f\rho_o - k_b\rho_r \qquad \text{and} \qquad \frac{d\rho_o}{dt} = k_b\rho_r - k_f\rho_o \tag{19}$$

where k_f and k_b are the pseudo first order forward and backward rate constants respectively. These changes of the concentrations lead to the currents of redox pairs through the interface that can be expressed as [30, 31, 65]

$$\begin{aligned} \boldsymbol{\nu}\cdot\mathbf{J}_r &\equiv -\frac{d\rho_r}{dt} = k_b(t,\mathbf{x})\rho_r(t,\mathbf{x}) - k_f(t,\mathbf{x})\rho_o(t,\mathbf{x}), \quad \text{on} \quad (0,T]\times\Sigma, \\ \boldsymbol{\nu}\cdot\mathbf{J}_o &\equiv -\frac{d\rho_o}{dt} = -k_b(t,\mathbf{x})\rho_r(t,\mathbf{x}) + k_f(t,\mathbf{x})\rho_o(t,\mathbf{x}), \quad \text{on} \quad (0,T]\times\Sigma. \end{aligned} \tag{20}$$

Here the signs in front of the terms are selected to be consistent with the fact that unit vector $\boldsymbol{\nu}(\mathbf{x})$ on Σ points from the semiconductor to the electrolyte.

The current from the semiconductor to the electrolyte $\boldsymbol{\nu}\cdot\mathbf{J}_n$, through the transfer of electrons to the electrolyte, is proportional to the concentration of the electrons on Σ_- and the concentration of the oxidants on Σ_+. The current for the backward process $\boldsymbol{\nu}\cdot\mathbf{J}_p$, is proportional to the concentration of the holes on Σ_- and the concentration of the reductant on Σ_+. More precisely, we have

$$\boldsymbol{\nu}\cdot\mathbf{J}_n = k_{et}(\mathbf{x})(\rho_n-\rho_n^e)\rho_o(t,\mathbf{x}),\quad \text{and},\quad \boldsymbol{\nu}\cdot\mathbf{J}_p = k_{ht}(\mathbf{x})(\rho_p-\rho_p^e)\rho_r(t,\mathbf{x}),\quad \text{on}\ \ (0,T]\times\Sigma. \tag{21}$$

Here the charge transfer rate constants k_{et} and k_{ht} are related to the reactions between electrons (n) and oxidants (o) and the reactions between holes (p) and reductants (r) respectively. The value of these parameters can be calculated approximately from the first principles of physical chemistry [5, 30, 31, 40, 48, 49, 50, 65, 68, 69, 70, 71, 72, 73, 84, 93]. Theoretical analysis shows that both parameters can be approximately treated as constant even though they could depend on the electric potential in specific situations. We reserve further investigation on this issue to future publications.

Following [30, 31, 65], we relate the reaction rate constants and the transfer rate constants by the following relations

$$k_f(t,\mathbf{x}) = k_{et}(\mathbf{x})(\rho_n-\rho_n^e),\quad \text{and},\quad k_b(t,\mathbf{x}) = k_{ht}(\mathbf{x})(\rho_p-\rho_p^e),\quad \text{on}\ \ (0,T]\times\Sigma. \tag{22}$$

We need to specify the interface condition for the electric potential as well. This is done by requiring Φ to be continuous across the interface and have continuous current. Let us denote by Σ_+ and Σ_- semiconductor and the electrolyte sides of Σ respectively, then the conditions on the electric potential are given by

$$[\Phi]_\Sigma \equiv \Phi_{|\Sigma_-} - \Phi_{|\Sigma_+} = 0,\qquad [\epsilon_r\frac{\partial\Phi}{\partial\nu}]_\Sigma \equiv \epsilon_r^{\mathsf{E}}\frac{\partial\Phi}{\partial\nu}|_{\Sigma_-} - \epsilon_r^{\mathsf{S}}\frac{\partial\Phi}{\partial\nu}|_{\Sigma_+} = 0,\quad \text{on}\ \ (0,T]\times\Sigma. \tag{23}$$

The interface conditions (20), (21) and (23) can now be supplied to the mathematical models in the semiconductor (1) and the electrolyte (14), together with the boundary conditions, to get a complete description of the semiconductor-electrolyte system that starts with any initial state.

5 Numerical discretization

We have presented a complete mathematical model for the transport of charges in the system of semiconductor-electrolyte for solar cell simulations. We now present a numerical procedure to solve the system of equations.

5.1 Non-dimensionalization

We first introduce the following characteristic quantities in the simulation regarding the device and its physics. We denote by l^* the characteristic length scale of the device, t^* the

characteristic time scale, Φ^* the characteristic voltage and C^* the characteristic density. The values for these characteristic quantities are respectively,

$$\begin{array}{llll} l^* = 10^{-4} & [\text{cm}], & t^* = 10^{-12} & [\text{s}] \\ \Phi^* = U_{\mathcal{T}} & [\text{V}], & C^* = 10^{16} & [\text{cm}^{-3}]. \end{array} \tag{24}$$

We now rescale all the physical quantities. To avoid introducing new notations, we will use the same notation for a quantity and its rescaled version. We introduce

$$\begin{array}{ll} t = t/t^*, & x = x/l^* \\ D_x = D_x \dfrac{t^*}{l^{*2}}, & \mu_x = \mu_x \dfrac{t^*\Phi^*}{l^{*2}}, \quad x \in \{n,p,r,o\} \\ R_{np}(\rho_n,\rho_p) = \dfrac{t^*}{C^*} R_{np}(C^*\rho_n, C^*\rho_p), & G_{np} = \dfrac{t^*}{C^*} G_{np}, \\ R_{ro}(\rho_r,\rho_o) = \dfrac{t^*}{C^*} R_{ro}(C^*\rho_r, C^*\rho_o), & \\ C = C/C^*, & \widehat{C} = \widehat{C}/C^* \end{array} \tag{25}$$

and the rescaled Debye lengths $\lambda_{\mathsf{S}} = \dfrac{1}{l^*}\sqrt{\dfrac{\Phi^*\epsilon^{\mathsf{S}}}{q\rho_n^*}}$ and $\lambda_{\mathsf{E}} = \dfrac{1}{l^*}\sqrt{\dfrac{\Phi^*\epsilon^{\mathsf{E}}}{q\rho_n^*}}$. We can then rewrite the system of equations in rescaled (non-dimensionalized) form as

$$\begin{array}{lll} \partial_t\rho_n - \nabla\cdot(D_n\nabla\rho_n - \mu_n\rho_n\nabla\Phi) = R_{np}(\rho_n,\rho_p) + \gamma G_{np}, & \text{in} & (0,T]\times\Omega_{\mathsf{S}}, \\ \partial_t\rho_p - \nabla\cdot(D_p\nabla\rho_p + \mu_p\rho_p\nabla\Phi) = R_{np}(\rho_n,\rho_p) + \gamma G_{np}, & \text{in} & (0,T]\times\Omega_{\mathsf{S}}, \\ -\nabla\cdot\lambda_{\mathsf{S}}^2\nabla\Phi = C + \rho_p - \rho_n, & \text{in} & (0,T]\times\Omega_{\mathsf{S}} \\ \partial_t\rho_r - \nabla\cdot(D_r\nabla\rho_r - \mu_r\rho_r\nabla\Phi) = R_{ro}(\rho_r,\rho_o), & \text{in} & (0,T]\times\Omega_{\mathsf{E}}, \\ \partial_t\rho_o - \nabla\cdot(D_o\nabla\rho_o + \mu_o\rho_o\nabla\Phi) = R_{ro}(\rho_r,\rho_o), & \text{in} & (0,T]\times\Omega_{\mathsf{E}}, \\ -\nabla\cdot\lambda_{\mathsf{E}}^2\nabla\Phi = \widehat{C} + \alpha_o\rho_o - \alpha_r\rho_r, & \text{in} & (0,T]\times\Omega_{\mathsf{E}}. \end{array} \tag{26}$$

where the forms of the rescaled generation-recombination rates are not changed if we perform the rescaling $A_p = t^*{\rho_n^*}^2 A_p$, $A_n = t^*{\rho_n^*}^2 A_n$, $\tau_p = \tau_p/t^*$, $\tau_n = \tau_n/t^*$ and $\rho_i = \rho_i/C^*$.

In the same manner, if we define the rescaled quantities

$$\begin{array}{llll} k_{et} = k_{et}t^*C^*/l^*, & k_{ht} = k_{ht}t^*C^*/l^* & k_f = k_f t^*/l^*, & k_b = k_b t^*/l^* \\ \rho_n^e = \rho_n^e/C^*, & \rho_p^e = \rho_p^e/C^*, & \rho_r^\infty = \rho_r^\infty/C^*, & \rho_o^\infty = \rho_o^\infty/C^* \\ v_n = v_n t^*/l^*, & v_p = v_p t^*/l^* & & \\ \varphi_{bi} = \varphi_{bi}/\Phi^*, & \varphi_{app} = \varphi_{app}/\Phi^*, & \varphi_{Schottky} = \varphi_{Schottky}/\Phi^*, & \\ \varphi_{bi}^{\mathsf{E}} = \varphi_{bi}^{\mathsf{E}}/\Phi^*, & \varphi_{app}^{\mathsf{E}} = \varphi_{app}^{\mathsf{E}}/\Phi^*, & & \end{array} \tag{27}$$

the rescaled boundary and interface conditions take exactly the same forms as those defined in (7), (12), (20), (21), and (23).

5.2 Time-dependent discretization

We discretize the systems of equations by standard finite difference method in both spatial and temporal variables. In the spatial variable, we employed a classical upwind discretization

of the advection terms (such as $\nabla\Phi\cdot\nabla\rho_n$) to ensure the stability of the scheme. The reaction-drift-diffusion-Poisson system of equations (26) are nonlinear equations that are posed in different spatial domains and then coupled through the interface conditions (20), (21), and (23). To avoid solving nonlinear system of equations in each time step, we employ the forward Euler scheme for the temporal variable. Since this is a first order scheme and is explicit, we do not need to perform any nonlinear solve in the solution process, as long as we can supply the right initial conditions. We are aware that there are many efficient solvers for similar problems that have been developed [57, 91]. To solve stationary problems, we can evolve the system for a long time so that the system reaches its stationary state. We use the magnitude of the relative L^2 update of the solution as the stopping criteria. An alternative, in fact more efficient, way to solve the nonlinear system is the following iterative scheme.

5.3 Gummel-Schwarz iteration for stationary problem

The method is to combine domain decomposition strategies with nonlinear iterative schemes. Here, we decompose the system naturally into two subsystems, the semiconductor system and the electrolyte system. We solve the two subsystem alternatively and couple them with the interface condition. This is the Schwarz decomposition strategy that have been used extensively in the literature; see [16, 66] for similar domain decomposition strategies in semiconductor simulation. To solve the nonlinear equations in each sub-problem, we adopt the Gummel iteration scheme [6, 9, 28, 43, 47]. This scheme decompose the drift-diffusion-Poisson system into a drift-diffusion part and a Poisson part and then solve the two parts alternatively. The coupling then come from the source term in the Poisson equation. Our algorithm, in the form of solving the stationary problem, takes the following form.

Gummel-Schwarz Algorithm.

[1] Gummel step $k=0$, construct initial guess $(\rho_n^0, \rho_p^0, \rho_r^0, \rho_o^0)$

[2] Gummel step $k \geq 1$

- Solve the Poisson problem for Φ^k in $\Omega_{\mathsf{E}} \cup \Omega_{\mathsf{S}}$ using the densities $\rho_n^{k-1}, \rho_p^{k-1}, \rho_r^{k-1}$ and ρ_o^{k-1}:

$$\begin{aligned}
&-\nabla\cdot\lambda_{\mathsf{S}}^2\nabla\Phi^k = C + \rho_p^{k-1} - \rho_n^{k-1}, && \text{in } \Omega_{\mathsf{S}}\\
&-\nabla\cdot\lambda_{\mathsf{E}}^2\nabla\Phi^k = \widehat{C} + \alpha_o\rho_o^{k-1} - \alpha_r\rho_r^{k-1}, && \text{in } \Omega_{\mathsf{E}}\\
&\Phi^k = \varphi_{bi} + \varphi_{app}, && \text{on } \Gamma_{\mathsf{S}o}\\
&\Phi^k = \varphi_{Schottky} + \varphi_{app}, && \text{on } \Gamma_{\mathsf{S}s}\\
&\Phi^k = \varphi^\infty, && \text{on } \Gamma_{\mathsf{E}}\\
&[\Phi^k]_\Sigma = 0, \quad [\epsilon_r\tfrac{\partial\Phi^k}{\partial\nu}]_\Sigma = 0, && \text{on } \Sigma.
\end{aligned} \tag{28}$$

- Solve for $\rho_n^k, \rho_p^k, \rho_r^k, \rho_o^k$ as limits of the iteration

  [i] Schwarz step $j=0$, construct guess $(\rho_n^{k,0}, \rho_p^{k,0}, \rho_r^{k,0}, \rho_o^{k,0})$

[ii] Schwarz step $j \geq 1$, solve *sequentially*

$$\begin{aligned}
&\nabla \cdot (-D_n \nabla \rho_n^{k,j} + \mu_n \rho_n^{k,j} \nabla \Phi^k) = R_{np}(\rho_n^{k,j}, \rho_p^{k,j}) + \gamma G_{np}(\mathbf{x}), && \text{in } \Omega_{\mathsf{S}} \\
&\nabla \cdot (-D_p \nabla \rho_p^{k,j} - \mu_p \rho_p^{k,j} \nabla \Phi^k) = R_{np}(\rho_n^{k,j}, \rho_p^{k,j}) + \gamma G_{np}(\mathbf{x}), && \text{in } \Omega_{\mathsf{S}} \\
&\rho_n^{k,j} = \rho_n^e(\mathbf{x}), \quad \rho_p^{k,j} = \rho_p^e(\mathbf{x}), && \text{on } \Gamma_{\mathsf{S}o} \\
&\boldsymbol{\nu} \cdot \mathbf{J}_n^{k,j} = v_n(\rho_n^{k,j} - \rho_n^e), \quad \boldsymbol{\nu} \cdot \mathbf{J}_p^{k,j} = v_p(\rho_p^{k,j} - \rho_p^e), && \text{on } \Gamma_{\mathsf{S}s} \\
&\boldsymbol{\nu} \cdot \mathbf{J}_n^{k,j} = k_{et}(\rho_n^{k,j} - \rho_n^e)\rho_o^{k,j-1}, \quad \boldsymbol{\nu} \cdot \mathbf{J}_p^{k,j} = k_{ht}(\rho_p^{k,j} - \rho_p^e)\rho_r^{k,j-1}, && \text{on } \Sigma
\end{aligned} \tag{29}$$

and

$$\begin{aligned}
&\nabla \cdot (-D_r \nabla \rho_r^{k,j} + \mu_r \rho_r^{k,j} \nabla \Phi^k) = R_{ro}(\rho_r^{k,j}, \rho_o^{k,j}), && \text{in } \Omega_{\mathsf{E}} \\
&\nabla \cdot (-D_o \nabla \rho_o^{k,j} - \mu_o \rho_o^{k,j} \nabla \Phi^k) = R_{ro}(\rho_r^{k,j}, \rho_o^{k,j}), && \text{in } \Omega_{\mathsf{E}} \\
&\rho_r^{k,j} = \rho_r^\infty(\mathbf{x}), \quad \rho_o^{k,j} = \rho_o^\infty(\mathbf{x}), && \text{on } \Gamma_{\mathsf{E}} \\
&\boldsymbol{\nu} \cdot \mathbf{J}_r^{k,j} = k_{ht}(\rho_p^{k,j} - \rho_p^e)\rho_r^{k,j} - k_{et}(\rho_n^{k,j} - \rho_n^e)\rho_o^{k,j}, && \text{on } \Sigma \\
&\boldsymbol{\nu} \cdot \mathbf{J}_o^{k,j} = -k_{ht}(\rho_p^{k,j} - \rho_p^e)\rho_r^{k,j} + k_{et}(\rho_n^{k,j} - \rho_n^e)\rho_o^{k,j}, && \text{on } \Sigma.
\end{aligned} \tag{30}$$

[iii] If convergence criteria satisfied, stop; Otherwise, set $j = j + 1$ and go to [iii].

[3] If convergence criteria satisfied, stop; Otherwise, set $k = k + 1$ and go to step [2].

Note that since (29) and (30) are solved *sequentially*, we are able to replace the $\rho_n^{k,j-1}$ and $\rho_p^{k,j-1}$ terms in (30) in the boundary conditions on Σ with $\rho_n^{k,j}$ and $\rho_p^{k,j}$ respectively, although the replacement is not necessary for the convergence of the algorithm.

The advantage of this scheme lies in the fact that it avoids bad scaling between semiconductor and electrolyte. If the mathematical system is well-posed, the convergence of this iteration can be established following the lines of work in [52, 53, 54, 87]. The details will be in a future work. The main computational problem comes from the stiffness on the interface caused by the huge contrast of the PDE systems on both sides of the interface.

6 Numerical simulations

In this section, we present some numerical simulations for the semiconductor-electrolyte system. For the simplicity of numerical implementation, we assume some symmetry in the system so that we can reduce the problem to one-dimension. We show in Fig. 2 two typical two-dimensional systems where such dimension reductions can be performed. In the first

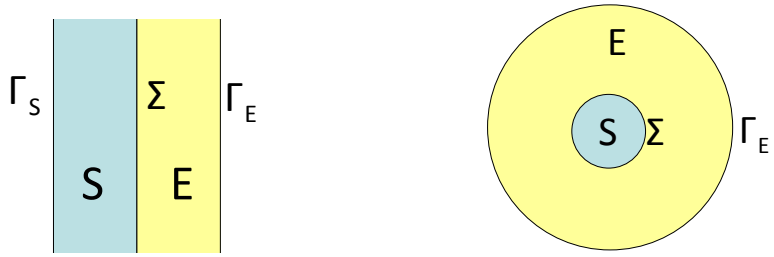

Figure 2: Two typical settings for semiconductor-electrolyte systems in dimension two. The semiconductor S and the electrolyte are separated by the interface Σ.

case, if we assume the system is invariant in the y-direction, then we have a one-dimensional

system in the x-direction. In the second setting, we have a radially symmetric system that is invariant in the angular direction in the polar coordinate. The system can then be regarded as a one-dimensional system in the radial direction. The form of the semiconductor equation in polar coordinates is very similar to the original equations, except that the current terms have to be replaced by

$$\begin{aligned}\nabla\cdot\mathbf{J}_n &= -\frac{1}{r}\big(\frac{\partial}{\partial r}(D_n r\frac{\partial\rho_n}{\partial r})+\frac{\partial}{\partial\theta}(\frac{D_n}{r}\frac{\partial\rho_n}{\partial\theta})\big)+\frac{1}{r}\big(\frac{\partial}{\partial r}(\mu_n\rho_n r\frac{\partial\Phi}{\partial r})+\frac{\partial}{\partial\theta}(\frac{\mu_n\rho_n}{r}\frac{\partial\Phi}{\partial\theta})\big),\\ \nabla\cdot\mathbf{J}_p &= -\frac{1}{r}\big(\frac{\partial}{\partial r}(D_p r\frac{\partial\rho_p}{\partial r})+\frac{\partial}{\partial\theta}(\frac{D_p}{r}\frac{\partial\rho_p}{\partial\theta})\big)-\frac{1}{r}\big(\frac{\partial}{\partial r}(\mu_p\rho_p r\frac{\partial\Phi}{\partial r})+\frac{\partial}{\partial\theta}(\frac{\mu_p\rho_p}{r}\frac{\partial\Phi}{\partial\theta})\big).\end{aligned} \tag{31}$$

where r and θ are the radial and angular variable respectively. Similar changes have to be applied to the electrolyte equations as well. We omit these new expressions here to save space.

There are many physical parameters in the mathematical models that we have introduced. The values of many parameters depend on the materials used. We list in Tab. 1 the values that we use in the simulations. All those physical parameters can be tuned to more realistic ones by careful calibration.

Parameter	value	unit	Parameter	value	unit
q	1.6×10^{-19}	[A s]	k_B	$8.62\times10^{-5}\ q$	[J K^{-1}]
ϵ_0	8.85×10^{-14}	[A s V^{-1} cm^{-1}]	ϵ_r^{S}	11.9	
μ_n	1500	[cm^2 V^{-1} s^{-1}]	μ_p	450	[cm^2 V^{-1} s^{-1}]
τ_n	1×10^{-6}	[s]	τ_p	1×10^{-5}	[s]
A_n	2.8×10^{-31}	[cm^6 s^{-1}]	A_p	9.9×10^{-32}	[cm^6 s^{-1}]
N_c	2.80×10^{19}	[cm^{-3}]	N_v	1.04×10^{19}	[cm^{-3}]
v_n	5×10^6	[cm s^{-1}]	v_p	5×10^6	[cm s^{-1}]
Φ_m	2.4	[V]	χ	1.2	[V]
k_{et}	1×10^{-21}	[cm^4 s^{-1}]	k_{ht}	1×10^{-17}	[cm^4 s^{-1}]
μ_o	2×10^{-1}	[cm^2 V^{-1} s^{-1}]	μ_r	0.5×10^{-1}	[cm^2 V^{-1} s^{-1}]
ϵ_r^{E}	1000		G_0	1.2×10^{17}	[cm^{-2}s^{-1}]

Table 1: Values of physical parameters used in the numerical simulations. The numbers are given in unit of cm, s, V, A. These are rough numbers taken from [3, 8, 42, 77, 90, 93] and references therein. Exact numbers for different materials can be found in these references.

To simplify the presentation, in all the simulations we have performed, we use an n-type semiconductor to construct the semiconductor-electrolyte system. The mathematical framework we have presented and the numerical algorithm we coded, however, is not limited to this case. We also select the electrolyte such that the charge numbers $\alpha_r=\alpha_o=1$, and set the temperature of the system to be $\mathcal{T}=300K$.

The main quantities that we are interested in are densities of charges, electric field and current through the system. The total current in the semiconductor part is $\mathbf{J}=\mathbf{J}_n-\mathbf{J}_p$. From the drift-diffusion-Poisson equation (1), it is clear that when the system evolves into stationary state, $\nabla\cdot\mathbf{J}=0$, which implies that $\mathbf{J}$ is constant in the semiconductor. The equation (14) for the redox pair indicates that $\nabla\cdot(\mathbf{J}_r+\mathbf{J}_o)=0$ in stationary state. This

together with the fact that $\boldsymbol{\nu} \cdot (\mathbf{J}_r + \mathbf{J}_o) = 0$ on Σ_+ leads to the conclusion that $\mathbf{J}_r = -\mathbf{J}_o$ in the electrolyte. The total current throughout the device is thus given us

$$\mathbf{J}(\mathbf{x}) = \begin{cases} \mathbf{J}_n(\mathbf{x}) - \mathbf{J}_p(\mathbf{x}), & \mathbf{x} \in \mathsf{S} \\ \mathbf{J}_r(\mathbf{x}), & \mathbf{x} \in \mathsf{E} \end{cases} \tag{32}$$

We will perform simulations on two devices of different sizes:

Device I. The device is contained in $\Omega = (-1.0l^*, 1.0l^*)$ with the semiconductor $\Omega_{\mathsf{S}} = (-1.0l^*, 0)$ and $\Omega_{\mathsf{E}} = (0, 1.0l^*)$ separated by the interface Σ located at $x = 0$. The semiconductor boundary Γ_{S} is thus at the point $x = -1.0l^*$ while the electrolyte boundary Γ_{E} is at the point $x = 1.0l^*$.

Device II. The device is contained in $\Omega = (-0.2l^*, 0.2l^*)$ with the semiconductor $\Omega_{\mathsf{S}} = (-0.2l^*, 0)$ and $\Omega_{\mathsf{E}} = (0, 0.2l^*)$ separated by the interface Σ located at $x = 0$. The semiconductor boundary Γ_{S} is thus at the point $x = -0.2l^*$ while the electrolyte boundary Γ_{E} is at the point $x = 0.2l^*$.

The two devices are designed to minimic a large (Device I) and small (Device II) nano-to-micro scale solar cell building blocks. We performance several simulations on each device. The setup for the simulations and the results are summarized in Tab. 2.

Case		Device	Summary			
I	(a)	I	$\epsilon_r^{\mathsf{E}} = 1000$,	$\rho_r^\infty = 30.0C^*$,	$\rho_o^\infty = 29.0C^*$,	Fig. 3 ($\gamma = 0$) Fig. 4 ($\gamma = 1$)
	(b)	I	$\epsilon_r^{\mathsf{E}} = 1000$,	$\rho_r^\infty = 4.0C^*$,	$\rho_o^\infty = 5.0C^*$,	Fig. 5 ($\gamma = 0$) Fig. 6 ($\gamma = 1$)
	(c)	I	$\epsilon_r^{\mathsf{E}} = 100$,	$\rho_r^\infty = 4.0C^*$,	$\rho_o^\infty = 5.0C^*$,	Fig. 7 ($\gamma = 0$) Fig. 8 ($\gamma = 1$)
II	(a)	II	$\epsilon_r^{\mathsf{E}} = 100$,	$\rho_r^\infty = 35.0C^*$,	$\rho_o^\infty = 30.0C^*$,	Figs. 9 & 10 ($\gamma = 0$)
	(b)	II	$\epsilon_r^{\mathsf{E}} = 100$,	$\rho_r^\infty = 2.0C^*$,	$\rho_o^\infty = 3.0C^*$,	Figs. 11 & 12 ($\gamma = 1$)
II′	(a)	II	$\epsilon_r^{\mathsf{E}} = 1000$,	$\rho_r^\infty = 4.5C^*$,	$\rho_o^\infty = 5.0C^*$,	Fig. 13 ($\gamma = 0$) Fig. 14 ($\gamma = 1$)
	(b)	II	$\epsilon_r^{\mathsf{E}} = 1000$,	$\rho_r^\infty = 35.0C^*$,	$\rho_o^\infty = 30.0C^*$,	Fig. 15

Table 2: Summary of configurations for simulations performed in Section 6. In each group (I, II, or II′), we only list the parameters that are changed during different simulations ((a), (b) or (c)). Other general parameters are given in Tab. 1.

6.1 General dynamics of semiconductor-electrolyte systems

We now present simulation results on general dynamics of the semiconductor-electrolyte systems we constructed. We perform the simulations using the first system, i.e. Device I.

General parameters in the simulations are listed in Tab. 1. We considered three different cases.

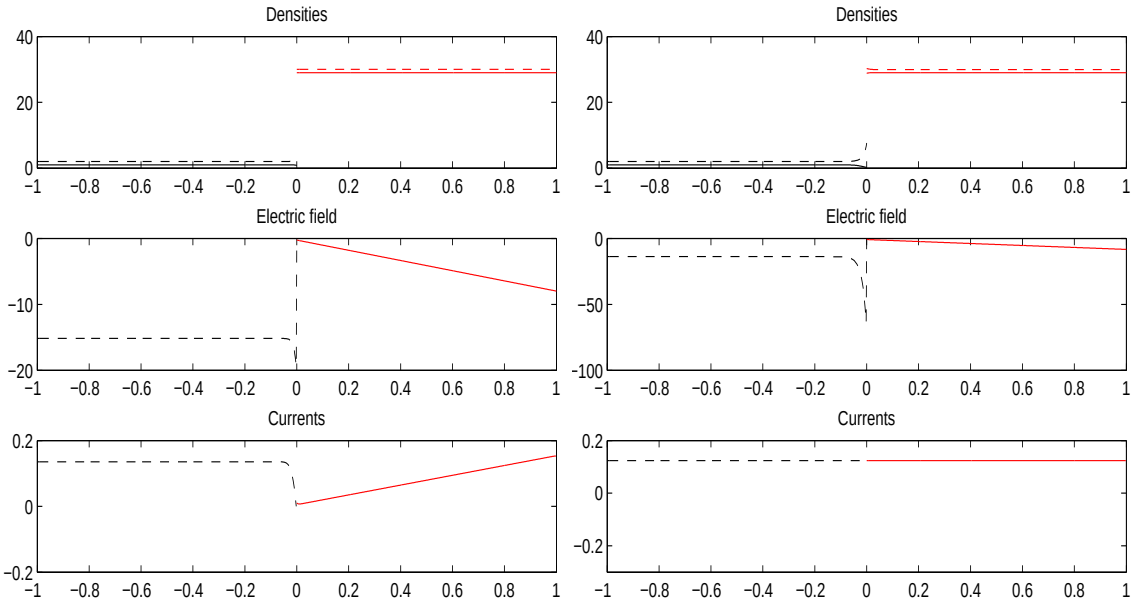

Figure 3: Case I (a) in dark environment ($\gamma = 0$). Left column: charge densities (black solid for ρ_p, black dashed for ρ_n, red solid for ρ_o and red dashed for ρ_r respectively), electric field and current distributions at time $t = 0.05t^*$; Right column: charge density, electric field and current distributions at stationary state.

Case I (a). In this simulation, we show typical dynamics of the semiconductor-electrolyte system in dark and illuminated cases. We consider the case when the densities of the reductant-oxidant pair are very high compared to the densities of the electron-hole pair. Precisely, we take $\rho_r^\infty = 30.0C^*$, $\rho_o^\infty = 29.0C^*$ where C^* is the characteristic density given in (24). The system starts from the initial conditions: $\rho_n^0 = 2C^*$ cm^{-3}, $\rho_p^0 = 1.0C^*$, $\rho_r^0 = \rho_r^\infty$, and $\rho_o^0 = \rho_o^\infty$. We first perform simulation for the dark case, i.e., when the parameter $\gamma = 0$ in the drift-diffusion system (1). In the left column of Fig. 3, we show the distributions of the charge densities, electric field and total currents in the semiconductor and the electrolyte at time $t = 0.05t^*$. The corresponding distributions at stationary state are shown in the right column.

We now repeat the simulation in the illuminated environment by setting the parameter $\gamma = 1$. In this case, the surface photon flux is set as $G_0 = 1.2 \times 10^{17}$ cm^{-2}s^{-1} to mimic a Air Mass 1.5 solar spectral irradiance. The simulation results are presented in Fig. 4. In both the dark and illuminated cases shown here, the applied potential bias is $19.3\Phi^* \approx 0.5$V, and Ohmic contact (i.e. Dirichlet condition) is assumed at the left end of the semiconductor.

Case I (b). We now perform a set of simulations with the same parameters as those simulations in the previous numerical experiment but with a lower bulk reductant and oxidant pair densities: $\rho_r^\infty = 4.0C^*$, $\rho_o^\infty = 5.0C^*$. The initial conditions for the simulation

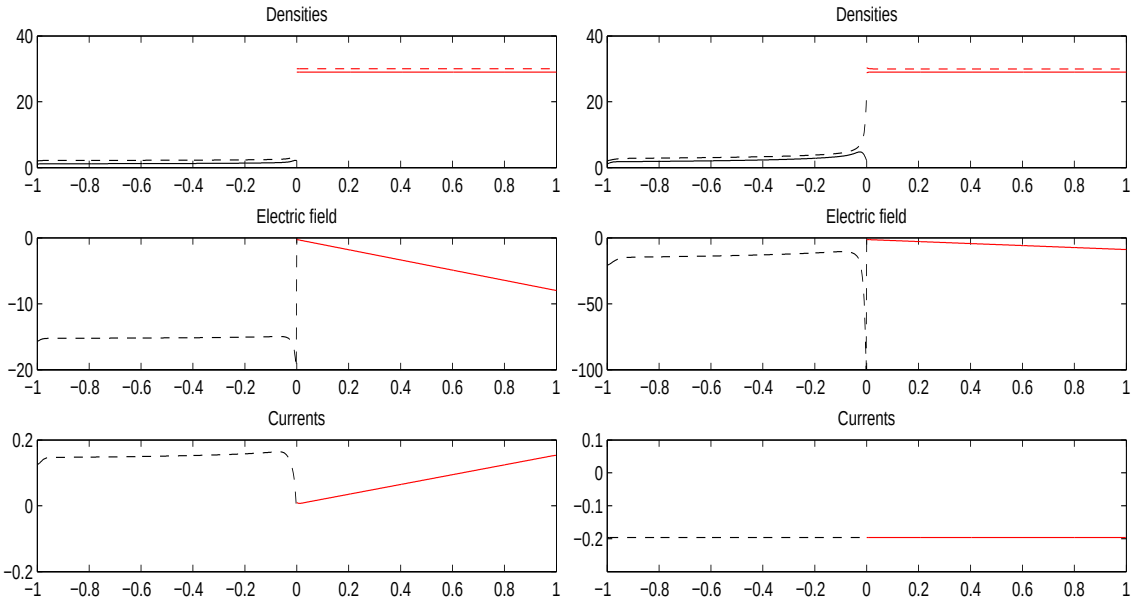

Figure 4: Case I (a) in illuminated environment ($\gamma = 1$). Left column: charge densities (black solid for ρ_p, black dashed for ρ_n, red solid for ρ_o and red dashed for ρ_r respectively), electric field and current distributions at time $t = 0.05t^*$; Right column: charge densities, electric field and current distributions at stationary state.

are: $\rho_n^0 = 2.5C^*$, $\rho_p^0 = 1.0C^*$, $\rho_r^0 = \rho_r^\infty$ and $\rho_o^0 = \rho_o^\infty$. The results in the dark and the illuminated environments are shown in Fig. 5 and Fig. 6 respectively. We observe from the comparison of Fig. 3 and Fig 4 with Fig. 5 and Fig. 6, that when all other factors are kept unchanged, lowering the density of the redox pair leads to significant change of the electric field across the device, especially at the semiconductor-electrolyte interface. The charge densities in the semiconductor also changes significantly. In both cases, however, the charge densities in the electrolyte, however, remain as almost constant across the electrolyte. There are two reasons for this. First, the charge densities in the electrolyte are significantly higher than those in the semiconductor (even in Case I (b)). Second, the relative dielectric constant of the electrolyte is much higher than that in the semiconductor, resulting in a relatively constant electric field inside the electrolyte. If we lower the relative dielectric function, we observe a significant variation in charge density distributions in the electrolyte as we can see from the next numerical simulation.

Case I (c). There is a large number of physical parameters in the semiconductor-electrolyte system that controls the dynamics of the system. To be specific, we show in this numerical simulation the impact of relative dielectric constant in the electrolyte ϵ_r^{E} on the system performance. The setup is exactly as in Case I (b) except that $\epsilon_r^{\mathsf{E}} = 100$ now. We perform simulations in both the dark and illuminated environments. We plot in Fig. 7 the densities, the electric field and the current distributions at time $t = 0.05t^*$ and stationary state. The corresponding results for illuminated case are shown in Fig. 8. It is not hard to observe the dramatic change in all the quantities shown after comparing Fig. 7 with Fig. 5, and Fig. 8

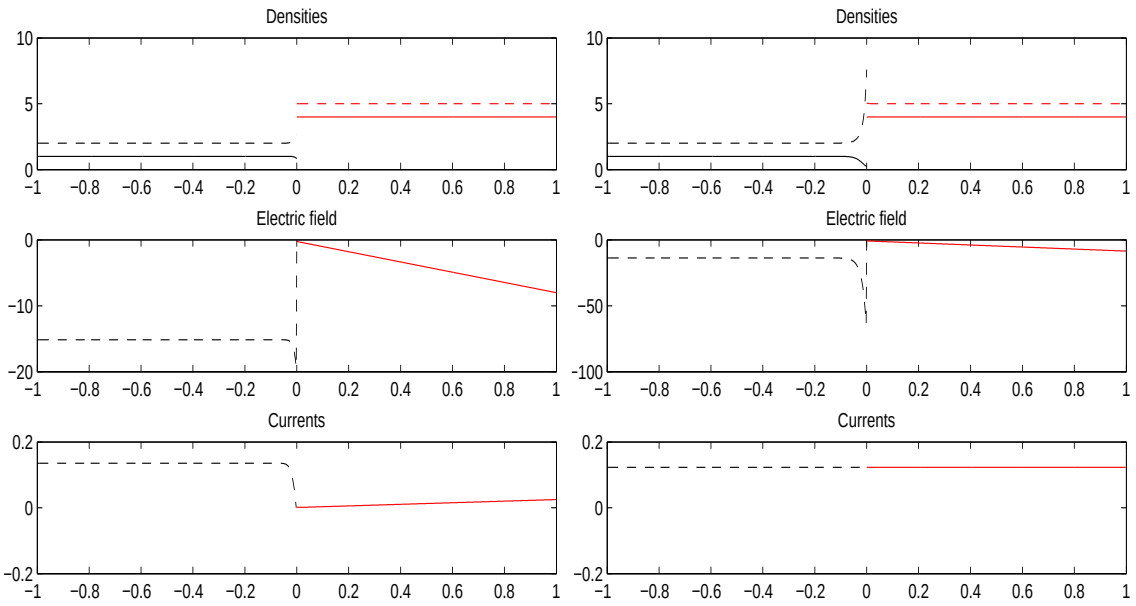

Figure 5: Case I (b) in dark environment ($\gamma = 0$). Left column: charge densities (black solid for ρ_p, black dashed for ρ_n, red solid for ρ_o and red dashed for ρ_r respectively), electric field and current distributions at time $t = 0.05t^*$; Right column: charge densities, electric field and current distributions at stationary state.

with Fig. 6. More detailed study of the parameter sensitivity problem will be reported elsewhere.

6.2 Comparison with Schottky approximation

In many simulations done for practical applications, it is assumed that the densities for the reductants and oxidants in the electrolyte are extremely high, so that reductant-oxidant dynamics changes very little compared to the electron-hole dynamics in the semiconductor. In this case, it is usually common to completely fix the electrolyte system and only evolve the electron-hole system. This is done by treating the electrolyte system as a Schottky contact and thus replacing the semiconductor-electrolyte interface conditions with Robin type of boundary conditions such as (12).

Our previous simulations, such as the ones shown in Fig. 3 and Fig. 4, indicate that such a simplification indeed can be accurate as the densities of the redox pair are roughly constant inside the electrolyte. We now present two simulations where we compare the simulations based on the our model of the whole system and the simulations based on Schottky approximation. Our simulations focus on Device II which is significantly smaller than Device I. Simulations for Device I show similar behaviors which we omit here to avoid repetition.

Due to the fact that the Schottky boundary condition contains no information on the parameters of the electrolyte system, it is impossible to make a direct quantitative comparison between the simulations. Instead, we will perform a comparison as follows. For each configuration of the electrolyte system, we select the parameters Φ_m, χ and E_g in the

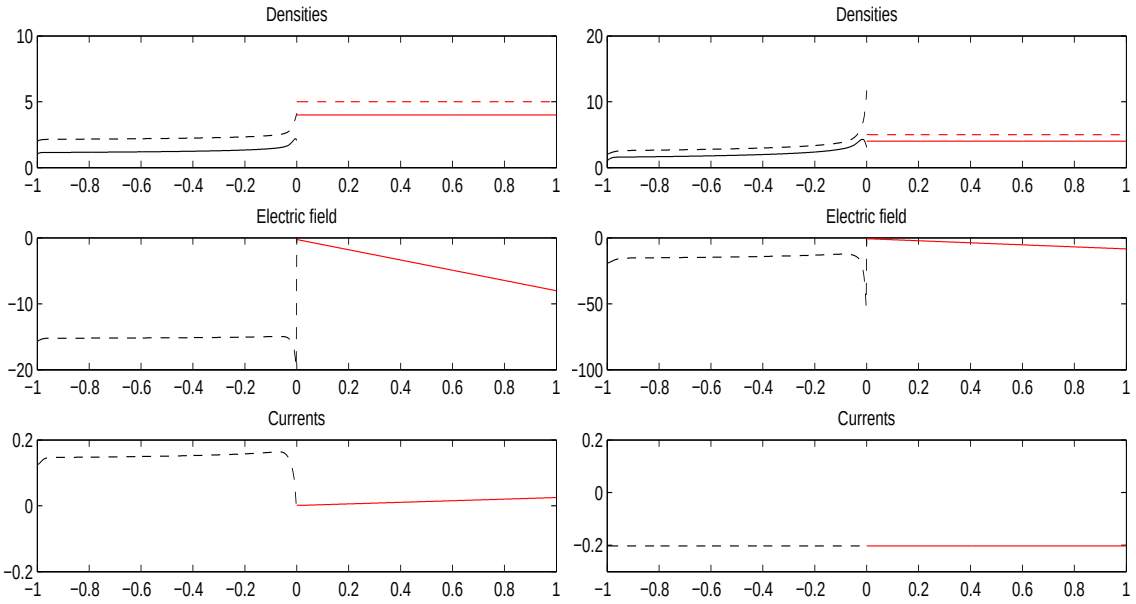

Figure 6: Case I (b) in illuminated environment ($\gamma = 1$). Left column: charge densities (black solid for ρ_p, black dashed for ρ_n, red solid for ρ_o and red dashed for ρ_r respectively), electric field and current distributions at time $t = 0.05t^*$; Right column: charge densities (black solid for ρ_p, black dashed for ρ_n, red solid for ρ_o and red dashed for ρ_r respectively), electric field and current distributions at stationary state.

Schottky potential (13) such that the total potential on the contact is equal to the bulk built-in of the electrolyte, i.e. $\varphi_{bi}^{\mathsf{E}}$ in (17).

We performed two sets of simulations on Device II. In the simulations with Schottky approximation, the Schottky contact locates at $x = 0$.

Case II (a). In the first set of simulations, we compare the whole system simulation with the Schottky approximation when the bulk reductant-oxidant pair density are more than 20 times higher than that of the electron-hole pair density. Precisely, the bulk densities for reductant and oxidant are respectively $\rho_r^\infty = 30.0\ C^*$ and $\rho_o^\infty = 35.0\ C^*$. The results in the semiconductor part are shown in Fig. 9 and those in the semiconductor part are shown in Fig. 10. We observed that in this case, the simulations with Schottky approximation are sufficiently close to the simulations with the whole system. This is to say that under such a case, replacing the electrolyte system with a Schottky contact provides a good approximation to the original system.

Case II (b). In the second set of simulations, we compare the two simulations when the bulk reductant-oxidant pair density is much lower than that in Case II(a). Precisely, $\rho_r^\infty = 2.0\ C^*$ and $\rho_o^\infty = 3.0\ C^*$. The results are shown in Fig. 11 (semiconductor part) and Fig. 12 (electrolyte part). While the qualitative behavior of the two systems are similar, the quantitative results are very different. We were not able to find a set of parameters in the boundary condition (12) that produce identical behavior of the semiconductor system. In

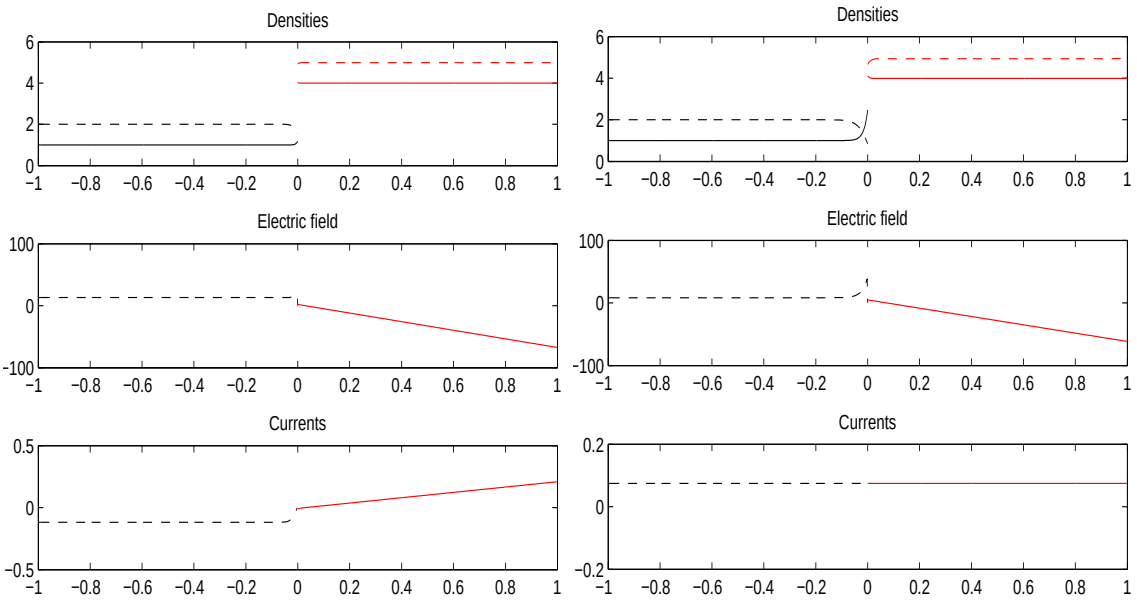

Figure 7: Case I (c) in dark environment ($\gamma = 0$). Shown are: charge densities (black solid for ρ_p, black dashed for ρ_n, red solid for ρ_o and red dashed for ρ_r respectively), electric field and current distributions at time $t = 0.05t^*$ (left column); and charge densities, electric field distributions at stationary state (right column).

this type of situations, simulation of the whole semiconductor-electrolyte system provides more accurate description of the physical process in the device.

The results above show that even though one can often replace the electrolyte system with a Schottky contact, modeling the whole semiconductor-electrolyte system offers more flexibilities in general. In the case when the bulk densities of the reductant and the oxidant are not extremely high compared to the densities of electrons and holes in the semiconductor, replacing the electrolyte system with a Schottky contact can cause large inaccuracy in predicted quantities.

6.3 Voltage-current characteristics

In the last set of numerical simulations, we study the voltage-current characteristics of the semiconductor-electrolyte system. We again focus on simulations with Device II, although we observe similar results for Device I.

Case II′ (a). We first compare simulations with forward potential bias with simulations with reverse potential bias in a dark environment. We take a device with low bulk reductant-oxidant densities ($\rho_r^\infty = 4.5\ C^*$, $\rho_o^\infty = 5.0\ C^*$) and high relative dielectric constant in electrolyte ($\epsilon_r^{\mathsf{E}} = 1000$). Shown on the left column of Fig. 13 are electron-hole and redox pair densities and the corresponding electric fields for applied forward potential bias of $35\Phi^* \approx 0.9V$. The same results for the applied reverse bias of $-35\Phi^*$ are presented on the right column of the same figure. Aside from the obvious differences in the densities and

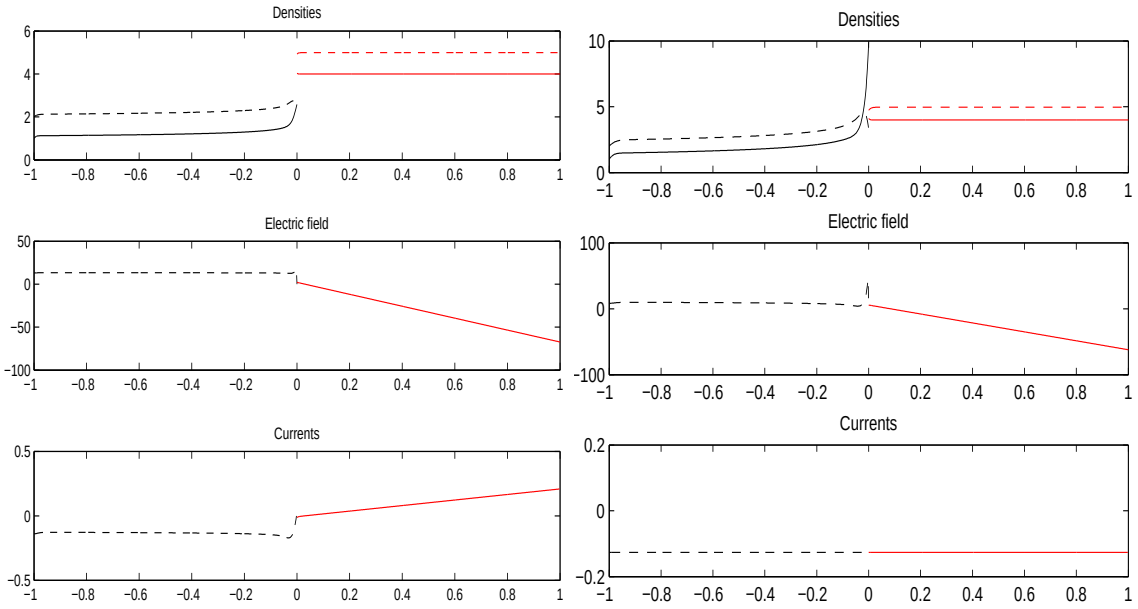

Figure 8: Case I (c) in illuminated environment ($\gamma = 1$). Shown are: charge densities (black solid for ρ_p, black dashed for ρ_n, red solid for ρ_o and red dashed for ρ_r respectively), electric field and current distributions at time $t = 0.05t^*$ (left column); and charge densities, electric field and current distributions at stationary state (right column).

electric field distributions, the currents through the system with forward and reverse biases are very different, as can be seen later on Fig. 15.

The simulations are repeated in Fig. 14 in the illuminated environment. It is clear from the plots in Fig. 13 and Fig. 14, illumination changes dramatically the distribution of charges (and thus the electric field) inside the device as we have seen in the previous simulations.

Case II′ (b). We now attempt to explore the whole current-voltage (I-V) characteristics of device II. To do that, we run the simulations for various different applied potentials and compute the current through the system under each applied potential. We plot the current data as a function of the applied potential to obtain the I-V curve of the system. The parameters are taken as $\rho_r^\infty = 35\ C^*$, $\rho_o^\infty = 30\ C^*$) and $\epsilon_r^{\mathsf{E}} = 1000$ to mimic these in realistic devices. We show in Fig. 15 the I-V curve obtained in both dark (line with stars) and illuminated (solid line with circles) environments. The applied potential bias lives in the range $[-1.5V,\ 1.9V]$ which is roughly $[-58.0\Phi^*,\ 73.5\Phi^*]$. The currents, with the unit of $10^{-8} q \frac{C^* l^*}{t^*} = 1.6$ mA cm^{-2}. The maximum power voltage The intersections of the dash-dotted vertical lines with the x-axis show the maximum power voltage ($\Phi_{\rm mp}$, red) and open circuit voltage ($\Phi_{\rm oc}$, blue) respectively. The intersections of the dashed horizontal lines with the y-axis show the maximum power current ($J_{\rm oc}$, red) and short circuit current ($J_{\rm sc}$, blue) respectively.

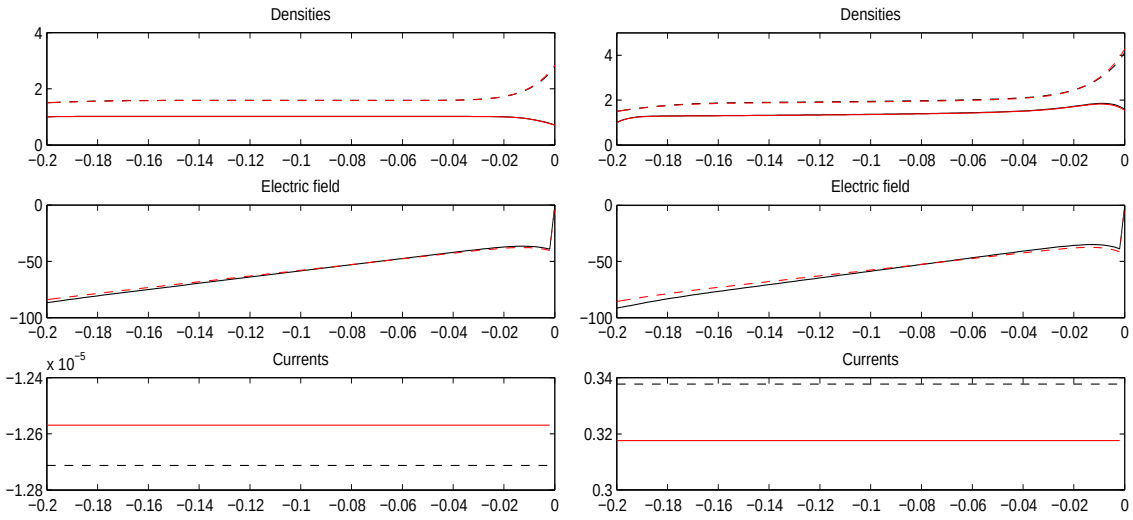

Figure 9: Case II (a): comparison between simulations from whole-system (red) and Schottky approximation (black) for Device II in dark ($\gamma = 0$, left column) and illuminated ($\gamma = 1$, right column) environments.

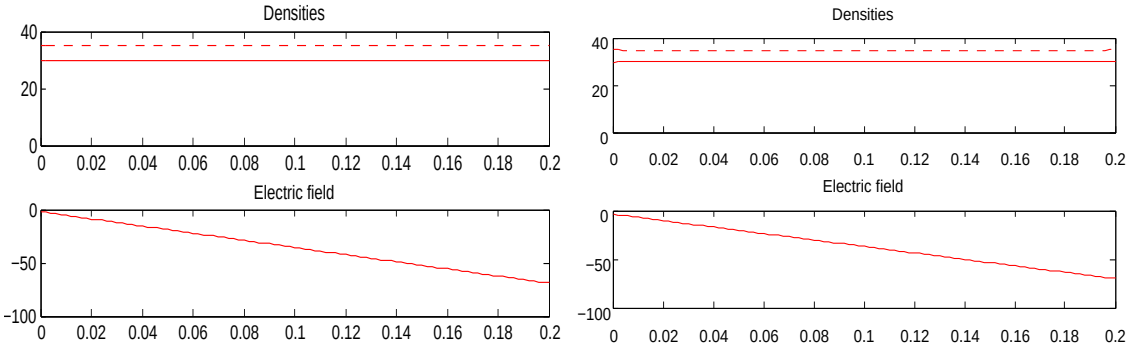

Figure 10: Case II (a): The electrolyte part of Fig. 9.

7 Conclusion and remarks

We have considered in this paper the mathematical modeling of semiconductor-electrolyte systems for applications in liquid-junction solar cells. We presented a complete mathematical model, a set of nonlinear partial differential equations with reactive interface conditions, for the simulation of such systems. Our model consists of a reaction-drift-diffusion-Poisson system that models the transport of electron-hole pairs in the semiconductor and an equivalent system that describes the transport of reductant-oxidant pairs in the electrolyte. The coupling of the two systems on the semiconductor-electrolyte interface is modeled with a set of reaction and current transfer type of interface conditions. We presented numerical procedures to solve both the time-dependent and stationary problem, for instance with Gummel-Schwarz double iteration. Some numerical simulations for one-dimensional devices are presented to illustrate the behavior of these devices.

Past study on the semiconductor-electrolyte system usually completely neglects the

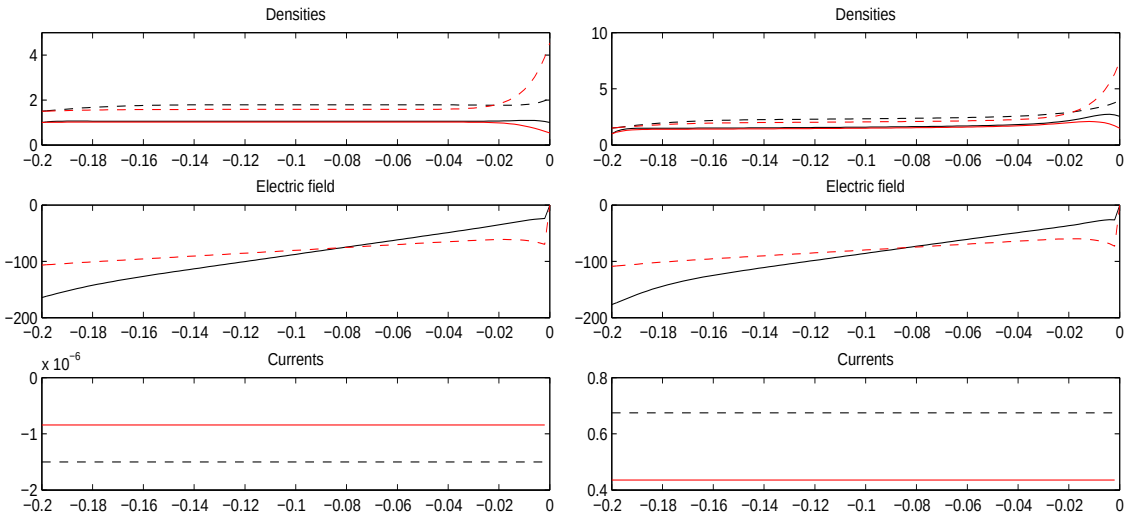

Figure 11: Case II (b): comparison between simulations from whole-system (red) and Schottky approximation (black) for Device II in dark ($\gamma = 0$, left column) and illuminated ($\gamma = 1$, right column) environments.

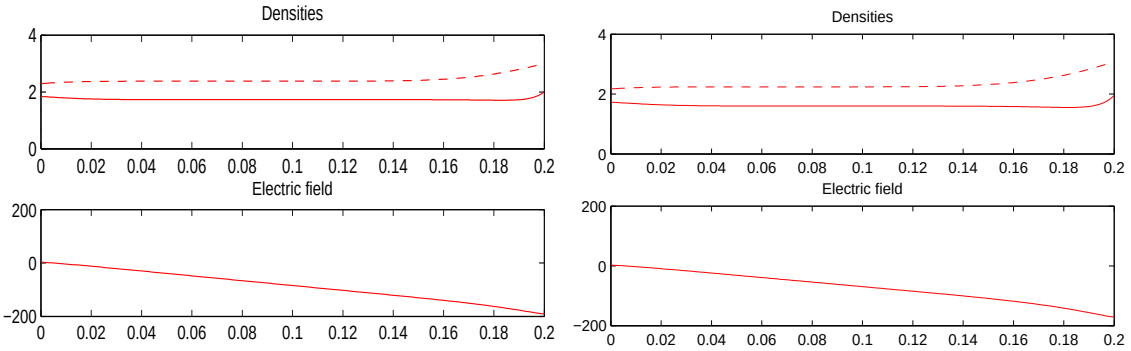

Figure 12: Case II (b): The electrolyte part of Fig. 11.

charge transfer processes in the electrolyte. The mathematical models developed thus only covers the semiconductor part with the interface effect modeled by a Robin type of boundary condition. The rational behind this simplification is the belief that the density of the reductant-oxidant pairs is so high compared to the density of the electron-hole pairs in the semiconductor such that the density of the redox pair would not be perturbed by the charge transfer process through the interface. While this might be a valid approximation in certain cases, it can certainly go wrong in other cases. For instance, it is generally observed that due to the strong electric field at the interface, there are dramatic change in the density of charges (both electron-hole and re-dox pairs) near the interface. What we presented, to our knowledge, is the first complete mathematical model for semiconductor-electrolyte solar cell systems that would allow us to accurately study the charge transfer process through the interface.

There are a variety of problems related to the model that we have constructed in this work that deserve thorough investigations. On the mathematical side, a detailed mathematical

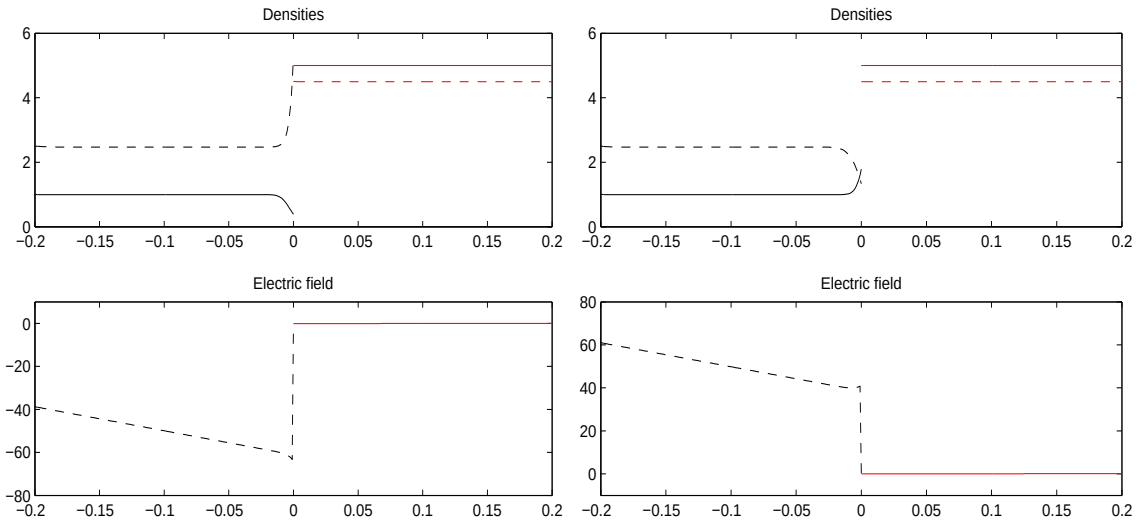

Figure 13: Case II′ (a) in dark ($\gamma = 0$) environment: comparison of charge densities (top) and the corresponding electric fields (bottom) in applied forward (left column) and reversed (right column) potential bias.

analysis on the well-posedness of the system is necessary. On the computational side, more detailed numerical analysis of the model, including convergence of the Gummel-Schwarz iteration, efficient high-order discretization and fast solution techniques, has to be studied. On the application side, it is important to calibrate the model parameters with experimental data that collected from real semiconductor-electrolyte solar cells. Once the aforementioned issues are addressed, we can use the model to help the design of more efficient solar cells by for instance optimizing the various model parameters. We are currently investigating several of these issues.

Acknowledgement

We would like to thank Professor Allen J. Bard and Charles B. Mullins for fruitful discussions on the current work. YH, IMG and HCL are supported by the NSF grants CHE 0934450 and DMS-0807712. KR is supported by NSF grant DMS-0914825.

References

[1] F. Alabau, *Structural properties of the one-dimensional drift-diffusion models for semiconductors*, Trans. Am. Math. Soc, 348 (1996), pp. 823–871.

[2] A. M. Anile, W. Allegretto, and C. Ringhofer, *Mathematical Problems in Semiconductor Physics*, Lecture Notes in Mathematics, Springer-Verlag, Berlin, 2003.

[3] A. J. Bard and L. R. Faulkner, *Electrochemical methods: fundamentals and applications*, Wiley, second ed., 2000.

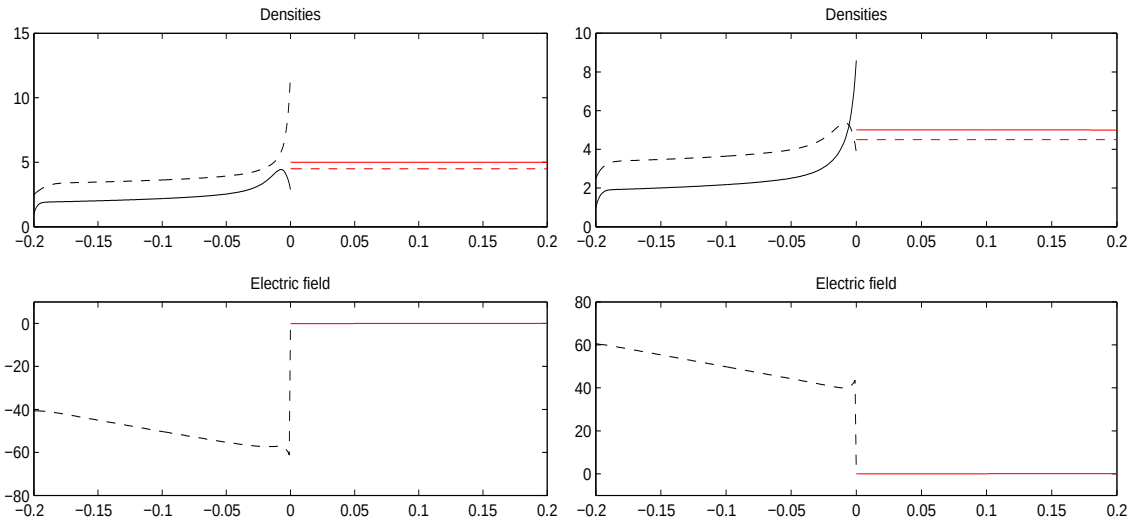

Figure 14: Case II′ (a) in illuminated ($\gamma = 1$) environment: comparison of charge densities (top) and the corresponding electric fields (bottom) in applied forward (left column) and reversed (right column) potential bias.

[4] S. Baumgartner and C. Heitzinger, *A one-level FETI method for the driftdiffusion-poisson system with discontinuities at an interface*, J. Comput. Phys., 243 (2013), pp. 74–86.

[5] J. Bell, T. Farrell, M. Penny, and G. Will, *A mathematical model of the semiconductor-electrolyte interface in dye sensitised solar cells*, in EMAC 2003 Proceedings, R. May and W. F. Blyth, eds., University of Technology, Sydney, Australia, 2003, Australian Mathematical Society, pp. 193–198.

[6] N. Ben Abdallah, M. J. Cáceres, J. A. Carrillo, and F. Vecil, *A deterministic solver for a hybrid quantum-classical transport model in nanoMOSFETs*, J. Comput. Phys., 228 (2009), pp. 6553–6571.

[7] N. Ben Abdallah and P. Degond, *On a hierarchy of macroscopic models for semiconductors*, J. Math. Phys., 37 (1996), pp. 3306–3333.

[8] K. F. Brennan, *The Physics of Semiconductors : with Applications to Optoelectronic Devices*, Cambridge University Press, New York, 1999.

[9] M. Burger and R. Pinnau, *A globally convergent Gummel map for optimal dopant profiling*, Math. Models Methods Appl. Sci., 19 (2009), pp. 769–786.

[10] J. A. Carrillo, I. Gamba, and C.-W. Shu, *Computational macroscopic approximations to the one-dimensional relaxation-time kinetic system for semiconductors*, Physica D, 146 (2000), pp. 289–306.

[11] J. A. Carrillo, I. M. Gamba, A. Majorana, and C.-W. Shu, *A WENO-solver for the transients of Boltzmann-Poisson system for semiconductor devices: performance and comparisons with Monte Carlo methods*, J. Comput. Phys., 184 (2003), pp. 498–525.

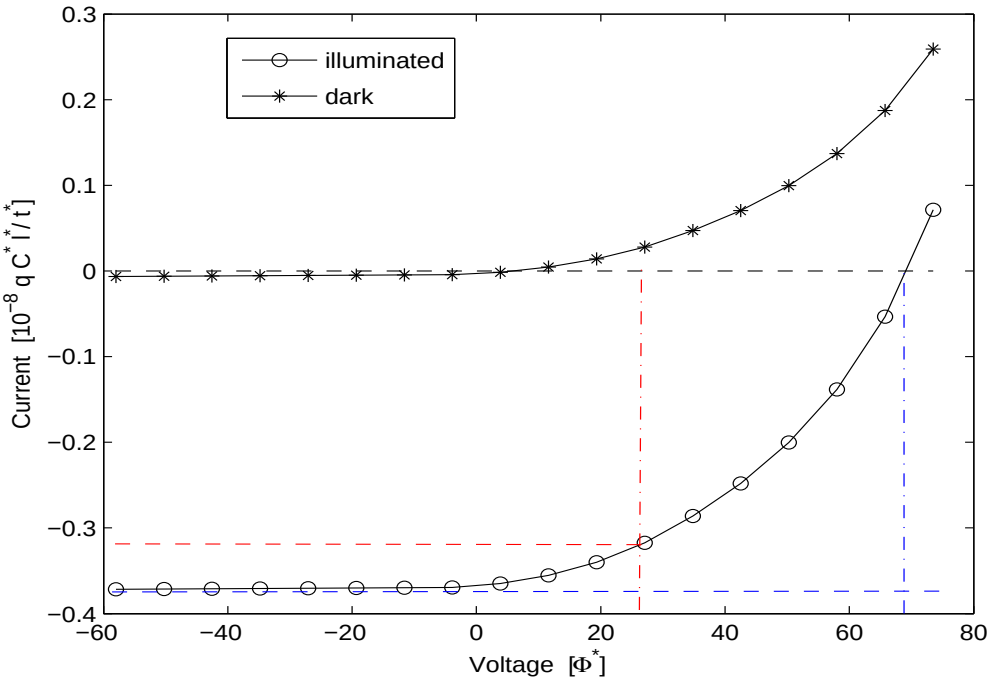

Figure 15: Case II′ (b): current-voltage (IV) curves for an n-type semiconductor-electrolyte system in dark (dotted line with circles) and illuminated (solid line with dots) environments. The intersections of the dash-dotted vertical lines with the x-axis show the maximum power voltage ($\Phi_{\rm mp}$, red) and open circuit voltage ($\Phi_{\rm oc}$, blue) respectively. The intersections of the dashed horizontal lines with the y-axis show the maximum power current ($J_{\rm oc}$, red) and short circuit current ($J_{\rm sc}$, blue) respectively.

[12] G. Cassano, C. de Falco, C. Giulianetti, and R. Sacco, *Numerical simulation of tunneling effects in nanoscale semiconductor devices using quantum corrected drift-diffusion models*, Computer Methods in Applied Mechanics and Engineering, 195 (2006), pp. 2193–2208.

[13] C. Cercignani, I. M. Gamba, and C. D. Levermore, *High field approximations to a Boltzmann-Poisson system and boundary conditions in a semiconductor*, Appl. Math. Lett., 10 (1997), pp. 111–118.

[14] ——, *A drift-collision balance asymptotic for a Boltzmann-Poisson system in bounded domains*, SIAM J. Appl. Math., 61 (2001), pp. 1932–1958.

[15] R.-C. Chen and J.-L. Liu, *An accelerated monotone iterative method for the quantum-corrected energy transport model*, J. Comput. Phys., 227 (2008), pp. 6226–6240.

[16] S. Chen, W. E, Y. Liu, and C.-W. Shu, *A discontinuous galerkin implementation of a domain decomposition method for kinetic-hydrodynamic coupling multiscale problems in gas dynamics and device simulations*, J. Comput. Phys., 225 (2007), pp. 1314–1330.

[17] Y. Cheng, I. Gamba, and K. Ren, *Recovering doping profiles in semiconductor devices with the Boltzmann-Poisson model*, J. Comput. Phys., 230 (2011), pp. 3391–3412.

[18] C. de Falco, M. Porro, R. Sacco, and M. Verri, *Multiscale modeling and simulation of organic solar cells*, Comput. Methods Appl. Mech. Engrg., 245 (2012), pp. 102–116.

[19] C. de Falco, R. Sacco, and M. Verri, *Analytical and numerical study of photocurrent transients in organic polymer solar cells*, Comput. Methods Appl. Mech. Engrg., 199 (2010), pp. 1722–1732.

[20] P. Degond and B. Niclot, *Numerical analysis of the weighted particle method applied to the semiconductor boltzmann equation*, Numer. Math., 55 (1989), pp. 599–618.

[21] A. Deinega and S. John, *Finite difference discretization of semiconductor drift-diffusion equations for nanowire solar cells*, Computer Physics Communications, 183 (2012), pp. 2128–2135.

[22] J. C. deMello, *Highly convergent simulations of transport dynamics in organic light-emitting diodes*, J. Comput. Phys., 181 (2002), pp. 564–576.

[23] C. R. Drago and R. Pinnau, *Optimal dopant profiling based on energy-transport semiconductor models*, Math. Models Meth. Appl. Sci., 18 (2008), pp. 195–241.

[24] B. Eisenberg, *Ionic channels: natural nanotubes described by the drift diffusion equations*, Superlattices and Microstructures, 27 (2000), pp. 545–549.

[25] W. R. Fawcett, *Liquids, Solutions, and Interfaces: From Classical Macroscopic Descriptions to Modern Microscopic Details*, Oxford University Press, New York, 2004.

[26] F. Filbet and S. Jin, *A class of asymptotic-preserving schemes for kinetic equations and related problems with stiff sources*, J. Comput. Phys., 229 (2010), pp. 7625–7648.

[27] J. M. Foley, M. J. Price, J. I. Feldblyum, and S. Maldonado, *Analysis of the operation of thin nanowire photoelectrodes for solar energy conversion*, Energy Environ. Sci., 5 (2012).

[28] S. Gadau and A. Jüngel, *A three-dimensional mixed finite-element approximation of the semiconductor energy-transport equations*, SIAM J. Sci. Comput., 31 (2008), pp. 1120–1140.

[29] M. Galler, *Multigroup equations for the description of the particle transport in semiconductors*, World Scientific, 2005.

[30] Y. Q. Gao, Y. Georgievskii, and R. A. Marcus, *On the theory of electron transfer reactions at semiconductor electrode/liquid interfaces*, J. Phys. Chem., 112 (2000), pp. 3358–3369.

[31] Y. Q. Gao and R. A. Marcus, *On the theory of electron transfer reactions at semiconductor electrode/liquid interfaces. II. A free electron model*, J. Phys. Chem., 112 (2000), pp. 6351–6360.

[32] A. Glitzky, *Analysis of electronic models for solar cells including energy resolved defect densities*, Math. Methods Appl. Sci., 34 (2011), pp. 1980–1998.

[33] T. Grasser, ed., *Advanced Device Modeling and Simulation*, World Scientific Press, Singapore, 2003.

[34] H. Haug and A.-P. Jauho, *Quantum Kinetics in Transport and Optics of Semiconductors*, Springer-Verlag, Berlin, 1996.

[35] T. L. Horng, T. C. Lin, C. Liu, and B. Eisenberg, *Pnp equations with steric effects: a model of ion flow through channels*, J Phys Chem B., 116 (2012), pp. 11422–11441.

[36] J. W. Jerome, *Analysis of Charge Transport: A Mathematical Study of Semiconductor Devices*, Springer-Verlag, Berlin, 1996.

[37] S. Jin and L. Pareschi, *Discretization of the multiscale semiconductor boltzmann equation by diffusive relaxation schemes*, J. Comput. Phys., 161 (2000), pp. 312–330.

[38] A. Jüngel, *Quasi-hydrodynamic Semiconductor Equations*, Birkhäuser, Basel, 2001.

[39] A. Jüngel, *Transport Equations for Semiconductors*, Springer, Berlin, 2009.

[40] P. V. Kamat, K. Tvrdy, D. R. Baker, and J. G. Radich, *Beyond photovoltaics: Semiconductor nanoarchitectures for liquid-junction solar cells*, Chem. Rev., 110 (2010), pp. 6664–6688.

[41] B. M. Kayes, H. A. Atwater, and N. S. Lewis, *Comparison of the device physics principles of planar and radial p-n junction nanorod solar cells*, J. Appl. Phys., 97 (2005). 114302.

[42] R. Kircher and W. Bergner, *Three-Dimensional Simulation of Semiconductor Devices*, Berkhäuser Verlag, Basel, 1991.

[43] A. A. Kulikovsky, *A more accurate Scharfetter-Gummel algorithm of electron transport for semiconductor and gas discharge simulation*, J. Comput. Phys., 119 (1995), pp. 149–155.

[44] D. Laser and A. J. Bard, *Semiconductor electrodes: IX digital simulation of the relaxation of photogenerated free carriers and photocurrents*, J. Electrochem. Soc.: Electrochemical Science and Technology, 123 (1976), pp. 1837–1842.

[45] ——, *Semiconductor electrodes: VII digital simulation of charge injection and the establishment of the space charge region in the absense of surface states*, J. Electrochem. Soc.: Electrochemical Science and Technology, 123 (1976), pp. 1828–1832.

[46] ——, *Semiconductor electrodes: VIII digital simulation of open-circuit photopotentials*, J. Electrochem. Soc.: Electrochemical Science and Technology, 123 (1976), pp. 1828–1837.

[47] W. R. Lee, S. Wang, and K. L. Teo, *An optimization approach to a finite dimensional parameter estimation problem in semiconductor device design*, J. Comput. Phys., 156 (1999), pp. 241–256.

[48] N. S. Lewis, *Photoeffects at the semiconductor/liquid interfaces*, Ann. Rev. Mater. Sci., 14 (1984), pp. 95–117.

[49] ——, *Mechanistic studies of light-induced charge separation at semiconductor/liquid interfaces*, Acc. Chem. Res., 23 (1990), pp. 176–183.

[50] ——, *Progress in understanding electron-transfer reactions at semiconductor/liquid interfaces*, J. Phys. Chem. B, 102 (1998), pp. 4843–4855.

[51] J. Li, C. Y., and Y. Liu, *Mathematical simulation of metamaterial solar cells*, Adv. Appl. Math. Mech., 3 (2011), pp. 702–715.

[52] P.-L. Lions, *On the Schwarz alternating method. I.*, in First International Symposium on Domain Decomposition Methods for Partial Differential Equations, SIAM, Philadelphia, PA, 1988, pp. 1–42.

[53] ——, *On the Schwarz alternating method. II. Stochastic interpretation and order properties.*, in Domain Decomposition Methods, SIAM, Philadelphia, PA, 1989, pp. 47–90.

[54] ——, *On the Schwarz alternating method. III. A variant for nonoverlapping subdomains.*, in Third International Symposium on Domain Decomposition Methods for Partial Differential Equations, SIAM, Philadelphia, PA, 1990, pp. 202–223.

[55] B. Liu, K. Nakata, X. Zhao, T. Ochiai, T. Murakami, and A. Fujishima, *Theoretical kinetic analysis of heterogeneous photocatalysis: The effect of surface trapping and bulk recombination through defects*, J. Phys. Chem. C, 115 (2011), pp. 16037–16042.

[56] W. Liu, *One-dimensional steady-state PoissonNernstPlanck systems for ion channels with multiple ion species*, J. Diff. Eqn., 246 (2009), pp. 428–451.

[57] W.-C. Lo, L. Chen, M. Wang, and Q. Nie, *A robust and efficient method for steady state patterns in reactiondiffusion systems*, J. Comput. Phys., 231 (2012), pp. 5062–5077.

[58] B. Lu, M. J. Holst, J. A. McCammon, and Y. C. Zhou, *Poissonnernstplanck equations for simulating biomolecular diffusionreaction processes I: Finite element solutions*, J. Comput. Phys., 229 (2010), pp. 6979–6994.

[59] B. Lu and Y. C. Zhou, *Poisson-Nernst-Planck equations for simulating biomolecular diffusion-reaction processes II: Size effects on ionic distributions and diffusion-reaction rates*, Biophysical Journal, 100 (2011), pp. 2475–2485.

[60] S. Mafé, J. Pellicer, and V. M. Aguilella, *A numerical approach to ionic transport through charged membranes*, J. Comput. Phys., 75 (1988), pp. 1–14.

[61] A. Majorana and R. Pidatella, *A finite difference scheme solving the Boltzmann-Poisson system for semiconductor devices*, J. Comput. Phys., 174 (2001), pp. 649–668.

[62] J. C. Manifacier, *Multiple steady state currentvoltage characteristics in driftdiffusion modelisation of N type and semi-insulating GaAs Gunn structures*, Solid-State Electronics, 54 (2010), pp. 1511–1519.

[63] P. A. Markowich, C. A. Ringhofer, and C. Schmeiser, *Semiconductor Equations*, Springer, New York, 1990.

[64] S. R. Mathur and J. Y. Murthy, *A multigrid method for the PoissonNernstPlanck equations*, International Journal of Heat and Mass Transfer, 52 (2009), pp. 4031–4039.

[65] R. Memming, *Semiconductor electrochemistry*, Wiley-VCH, 2001.

[66] S. Micheletti, A. Quarteroni, and R. Sacco, *Current-voltage characteristics simulation of semiconductor devices using domain decomposition*, J. Comput. Phys., 119 (1995), pp. 46–61.

[67] B. Niclot, P. Degond, and F. Poupaud, *Deterministic particle simulations of the Boltzmann transport equation of semiconductors*, J. Comput. Phys., 78 (1988), pp. 313–349.

[68] A. J. Nozik and R. Memming, *Physical chemistry of semiconductor-liquid interfaces*, J. Phys. Chem., 100 (1996), pp. 13061–13078.

[69] M. E. Orazem and J. Newman, *Mathematical modeling of liquid-junction photovoltaic cells I. governing equations*, J. Electrochem. Soc., 131 (1984), pp. 2569–2574.

[70] ——, *Mathematical modeling of liquid-junction photovoltaic cells II. effect of system parameters on current-potential curves*, J. Electrochem. Soc., 131 (1984), pp. 2574–2582.

[71] ——, *Mathematical modeling of liquid-junction photovoltaic cells III. optimization of cell configurations*, J. Electrochem. Soc., 131 (1984), pp. 2582–2589.

[72] M. Penny, T. Farrell, and C. Please, *A mathematical model for interfacial charge transfer at the semiconductor-dye-electrolyte interface of a dye-sensitised solar cell*, Solar Energy Materials and Solar Cells, 92 (2008), pp. 11–23.

[73] M. A. Penny, T. W. Farrell, G. D. Will, and J. M. Bell, *Modelling interfacial charge transfer in dye-sensitised solar cells*, J. Photochem. Photobiol. A, 164 (2004), pp. 41–46.

[74] G. Richardson, C. Please, J. Foster, and J. Kirkpatrick, *Asymptotic solution of a model for bilayer organic diodes and solar cells*, SIAM J. Appl. Math., 72 (2012), pp. 1792–1817.

[75] C. A. Ringhofer, *Computational methods for semiclassical and quantum transport in semiconductor devices*, Acta Numer., 6 (1997), pp. 485–521.

[76] A. Rossani, *A new derivation of the driftdiffusion equations for electrons and phonons*, Physica A: Statistical Mechanics and its Applications, 390 (2011), pp. 223–230.

[77] A. Schenk, *Advanced Physical Models for Silicon Device Simulation*, Springer-Verlag, Wien, 1998.

[78] D. Schroeder, *Modelling of Interface Carrier Transport for Device Simulation*, Springer-Verlag, Wien, 1994.

[79] Z. Schuss, B. Nadler, and R. S. Eisenberg, *Derivation of PNP equations in bath and channel from a molecular model*, Phys. Rev. E, 64 (2001). 036116.

[80] S. Selberherr, *Analysis and Simulation of Semiconductor Devices*, Springer-Verlag, Vienna, Austria, 1984.

[81] N. Seoane, A. J. García-Loureiro, K. Kalna, and A. Asenov, *Impact of intrinsic parameter fluctuations on the performance of HEMTs studied with a 3d parallel drift-diffusion simulator*, Solid-State Electronics, 51 (2007), pp. 481–488.

[82] S. Sho and S. Odanaka, *A quantum energy transport model for semiconductor device simulation*, J. Comput. Phys., 235 (2013), pp. 486–496.

[83] A. Singer and J. Norbury, *A Poisson-Nernst-Planck model for biological ion channels– An asymptotic analysis in a 3-D narrow funnel*, European J. Appl. Math., 19 (2008), pp. 541–560.

[84] D. Singh, X. Guo, J. Y. Murthy, A. Alexeenko, and T. Fisher, *Modeling of subcontinuum thermal transport across semiconductor-gas interfaces*, J. Appl. Phys., 106 (2009). 024314.

[85] H. Steinrück, *A bifurcation analysis of the one-dimensional steady-state semiconductor device equations*, SIAM J. Appl. Math., 49 (1989), pp. 1102–1121.

[86] P. Thum, T. Clees, G. Weyns, G. Nelissen, and J. Deconinck, *Efficient algebraic multigrid for migrationdiffusionconvectionreaction systems arising in electrochemical simulations*, J. Comput. Phys., 229 (2010), pp. 7260–7276.

[87] A. Toselli and O. B. Widlund, *Domain Decomposition Methods - Algorithms and Theory*, Springer-Verlag, 2005.

[88] M. J. Ward, L. G. Reyna, and F. M. Odeh, *Multiple steady-state solutions in a multijunction semiconductor device*, SIAM J. Appl. Math., 51 (1991), pp. 90–123.

[89] Y. Yamada, *Energy transport drift-diffusion model for submicrometer GaAs MESFETs*, Microelectronics Journal, 28 (1997), pp. 561–569.

[90] P. Y. Yu and M. Cardona, *Fundamentals of Semiconductors: Physics and Materials Properties*, Springer, Berlin, 3rd ed., 2003.

[91] S. Zhao, J. Ovadia, X. Liu, Y.-T. Zhang, and Q. Nie, *Operator splitting implicit integration factor methods for stiff reactiondiffusionadvection systems*, J. Comput. Phys., 230 (2011), pp. 5996–6009.

[92] Q. Zheng, D. Chen, and G.-W. Wei, *Second-order PoissonNernstPlanck solver for ion transport*, J. Comput. Phys., 230 (2011), pp. 5239–5262.

[93] H. Zhu, *Experimental and theoretical aspects of electrode/electrolyte interfaces*, PhD thesis, Case Western Reserve University, Cleveland, Ohio, 2010.